Electronic Supplementary Material (ESI) for Physical Chemistry Chemical Physics.

Supplementary Information for: Ab-initio calculations of temperature dependent electronic structure of inorganic halide perovskite materials

Milan Jocić* and Nenad Vukmirović†
Institute of Physics Belgrade, University of Belgrade, Pregrevica 118, 11080 Belgrade, Serbia

* milan.jocic@ipb.ac.rs
† nenad.vukmirovic@ipb.ac.rs

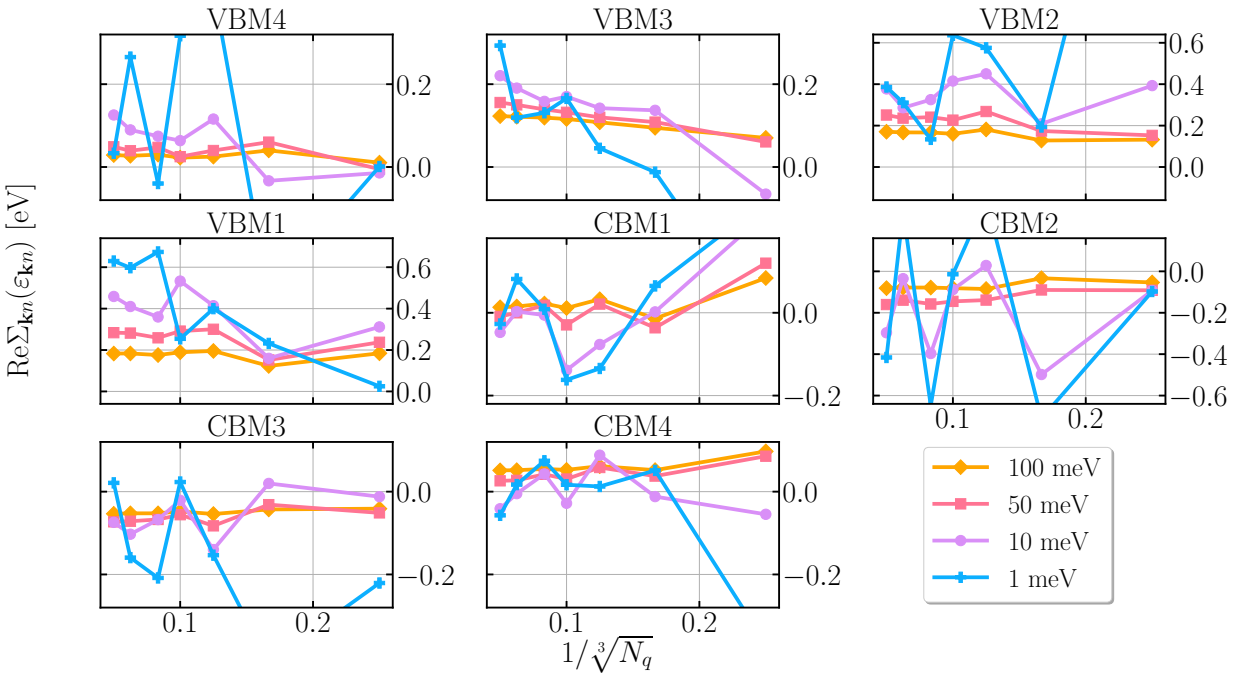

Fig. S1. The dependence of band energy renormalization in the OTMS approach on the number of q-points and energy level broadening parameter δ for $CsPbCl_3$ at $T = 400$ K.

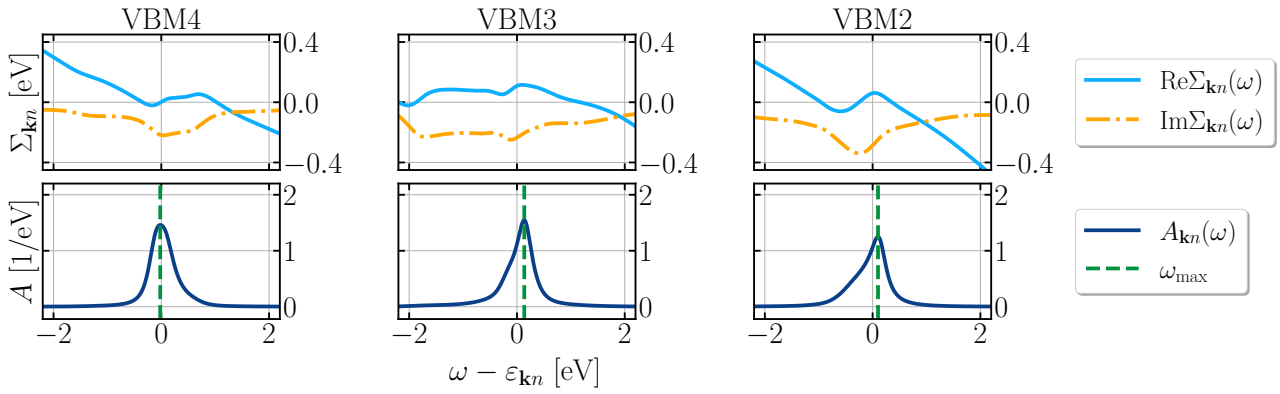

Fig. S2. The frequency dependence of the self-energy and the spectral function for bands VBM4, VBM3, and VBM2 at the R point in the case of $CsPbCl_3$ material at $T = 400$ K.

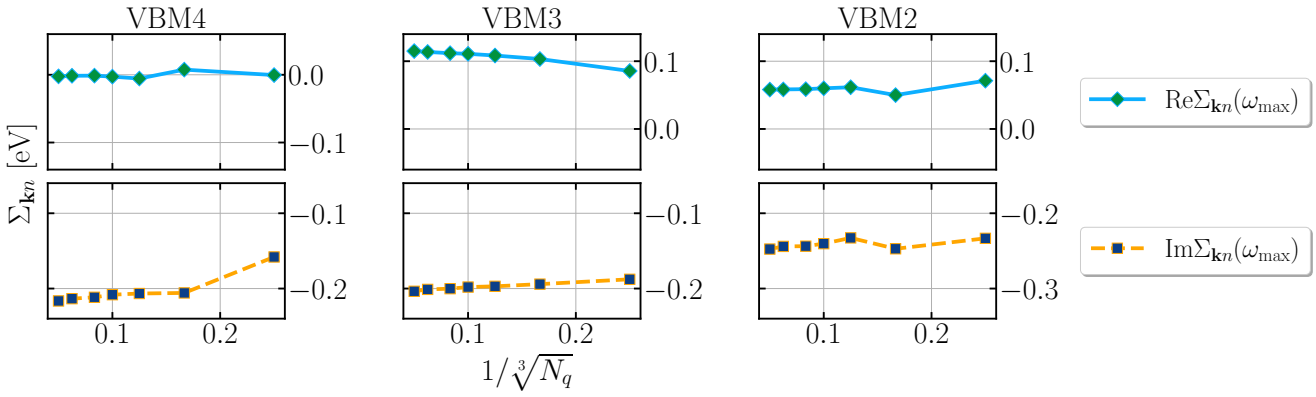

Fig. S3. The dependence of the real and imaginary part of self-energy at the renormalized energy on the size of the q-points grid. The results are presented for $CsPbCl_3$ material at $T = 400$ K for bands VBM4, VBM3, and VBM2 at the R point.

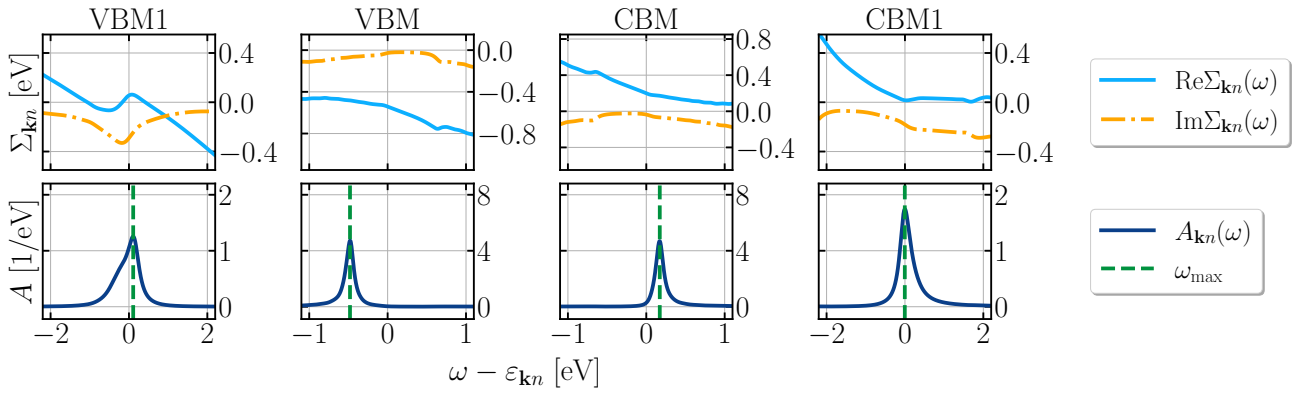

Fig. S4. The frequency dependence of the self-energy and the spectral function for bands VBM1, VBM, CBM and CBM1 at the R point in the case of $CsPbCl_3$ material at $T = 400$ K.

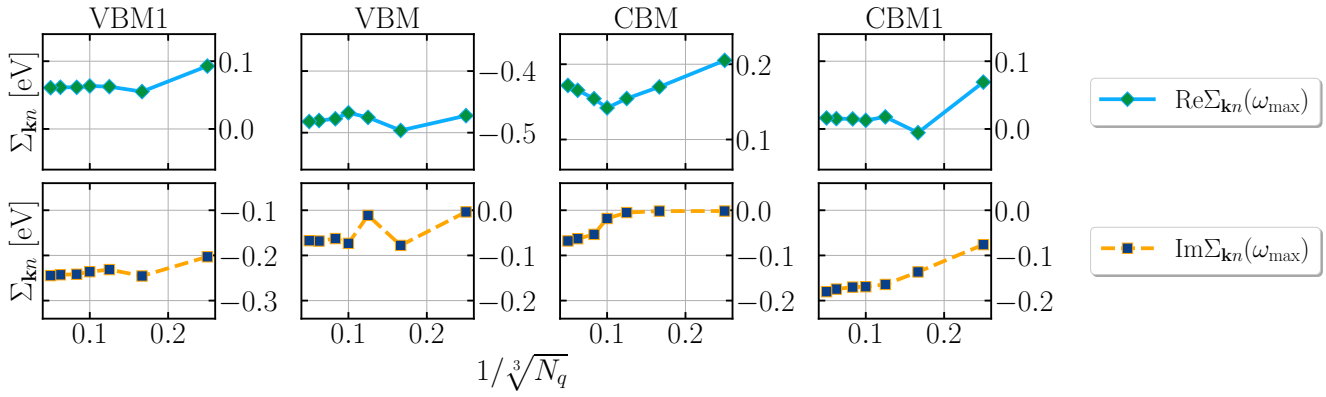

Fig. S5. The dependence of the real and imaginary part of self-energy at the renormalized energy on the size of the q-points grid. The results are presented for $CsPbCl_3$ material at $T = 400$ K for bands VBM1, VBM, CBM and CBM1 at the R point.

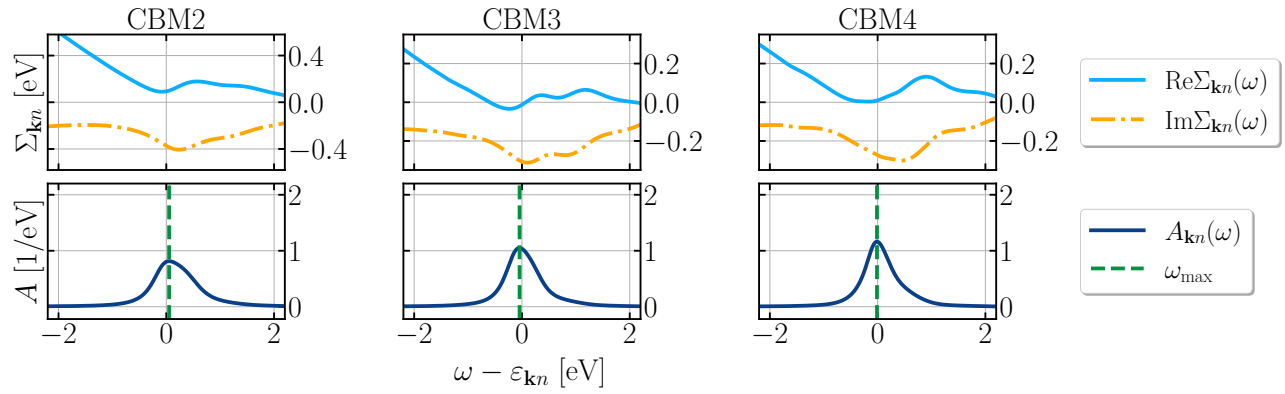

Fig. S6. The frequency dependence of the self-energy and the spectral function for bands CBM2, CBM3, and CBM4 at the R point in the case of $CsPbCl_3$ material at $T = 400$ K.

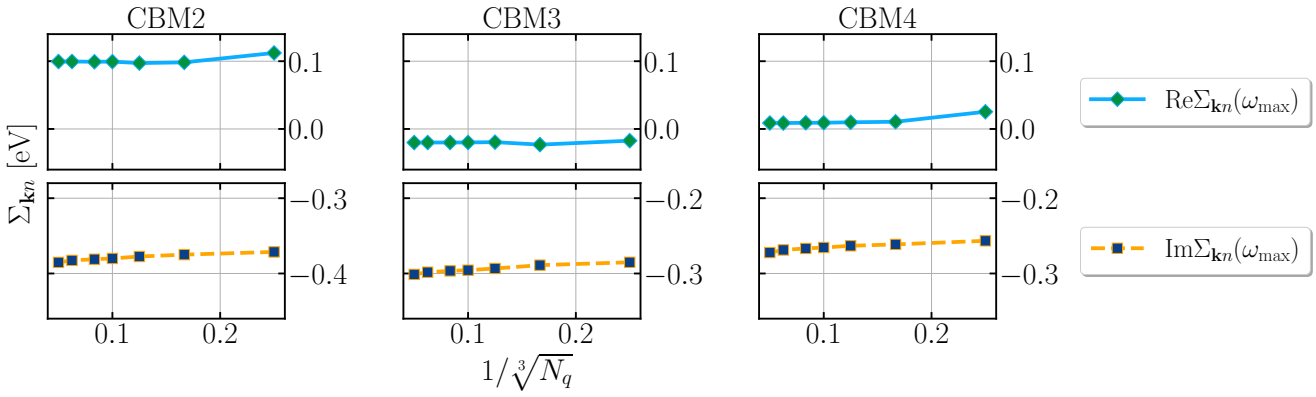

Fig. S7. The dependence of the real and imaginary part of self-energy at the renormalized energy on the size of the q-points grid. The results are presented for $CsPbCl_3$ material at $T = 400$ K for bands CBM2, CBM3, and CBM4 at the R point.

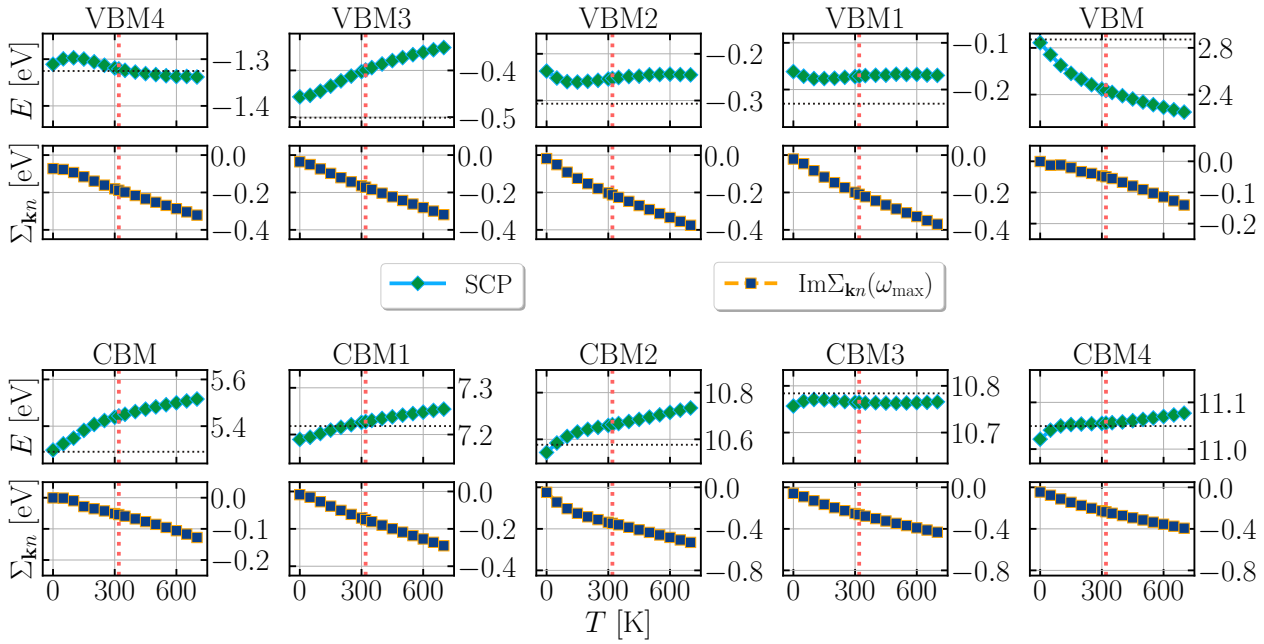

Fig. S8. Temperature dependence of the band energy and the imaginary part of the self-energy for VBM and VBMx (CBM and CBMx) bands (where $x = 1, 2, 3, 4$) calculated using the SCP approach. The results are shown for $CsPbCl_3$ at the R point. Vertical and horizontal dotted lines represent the temperature of the phase transition to cubic structure $T_c = 320$ K and band energy from PBE0 calculations, respectively.

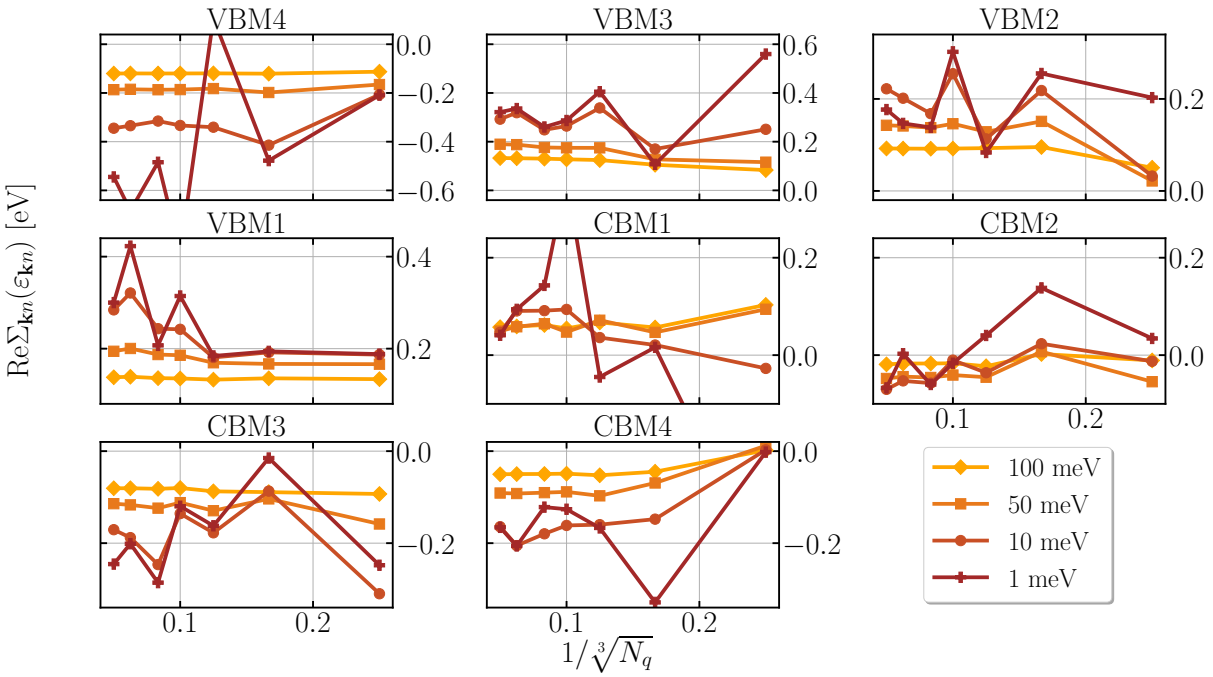

Fig. S9. The dependence of band energy renormalization in the OTMS approach on the number of q-points and energy level broadening parameter δ for $CsPbBr_3$ at $T = 400$ K.

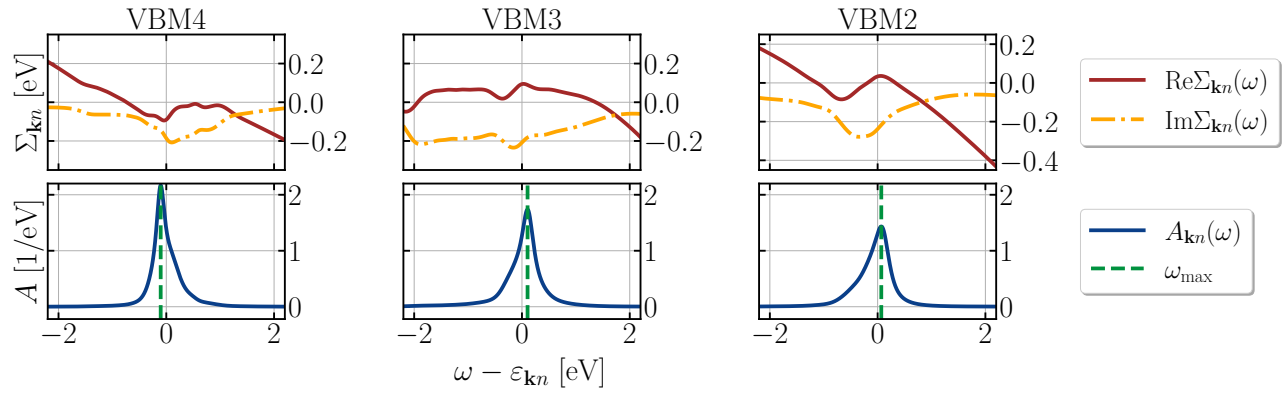

Fig. S10. The frequency dependence of the self-energy and the spectral function for bands VBM4, VBM3, and VBM2 at the R point in the case of $CsPbBr_3$ material at $T = 400$ K.

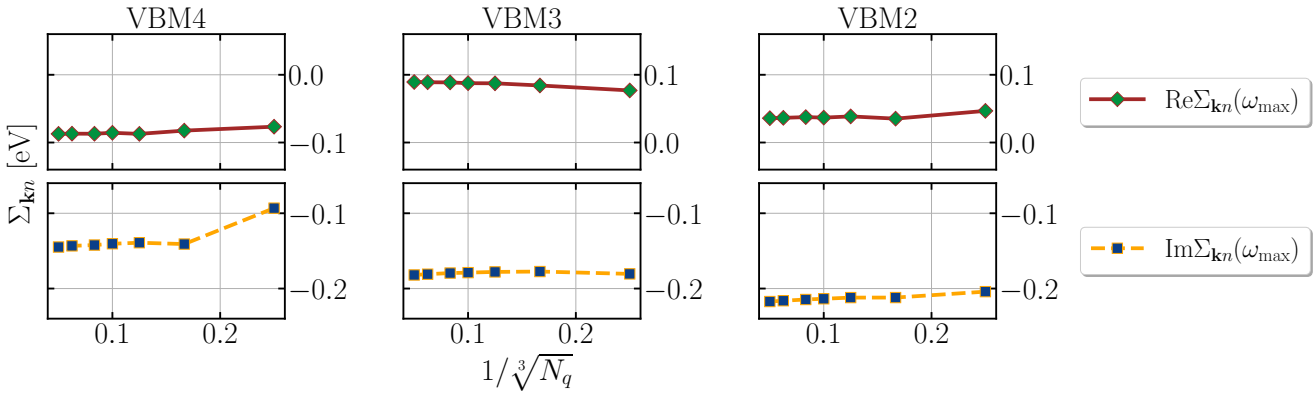

Fig. S11. The dependence of the real and imaginary part of self-energy at the renormalized energy on the size of the q-points grid. The results are presented for $CsPbBr_3$ material at $T = 400$ K for bands VBM4, VBM3, and VBM2 at the R point.

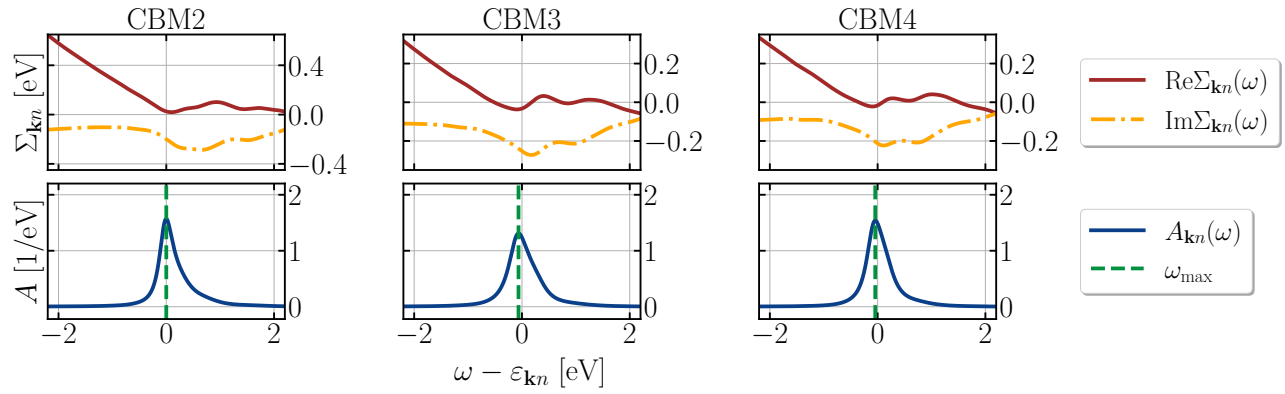

Fig. S12. The frequency dependence of the self-energy and the spectral function for bands CBM2, CBM3, and CBM4 at the R point in the case of $CsPbBr_3$ material at $T = 400$ K.

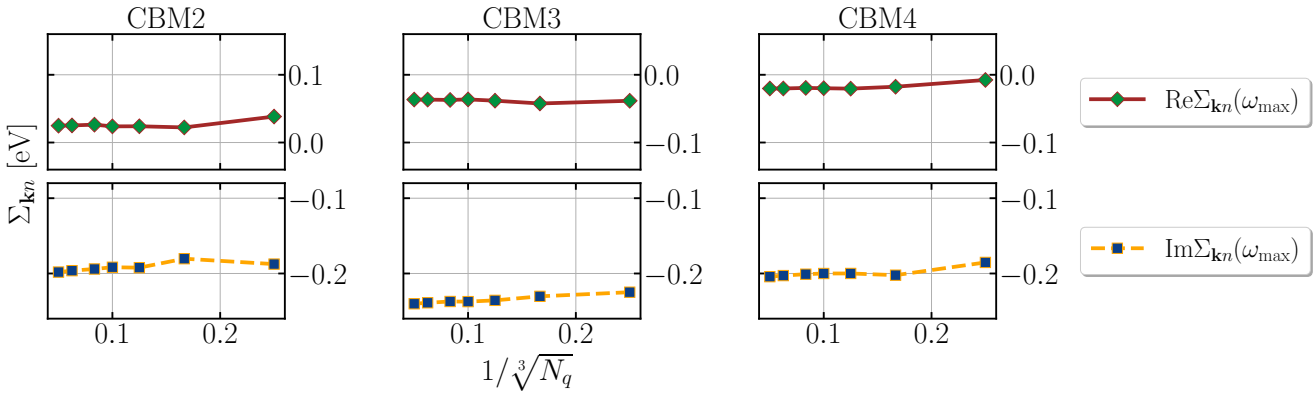

Fig. S13. The dependence of the real and imaginary part of self-energy at the renormalized energy on the size of the q-points grid. The results are presented for $CsPbBr_3$ material at $T = 400$ K for bands CBM2, CBM3, and CBM4 at the R point.

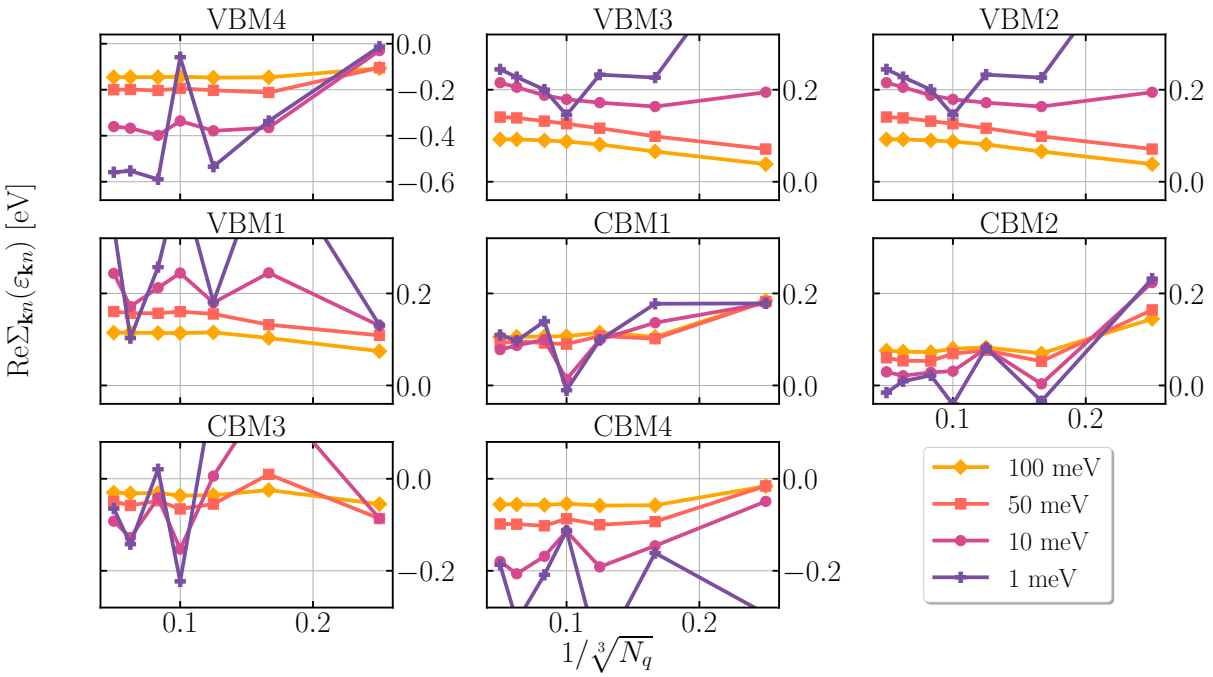

Fig. S14. The dependence of band energy renormalization in the OTMS approach on the number of q-points and energy level broadening parameter δ for $CsPbI_3$ at $T = 400$ K.

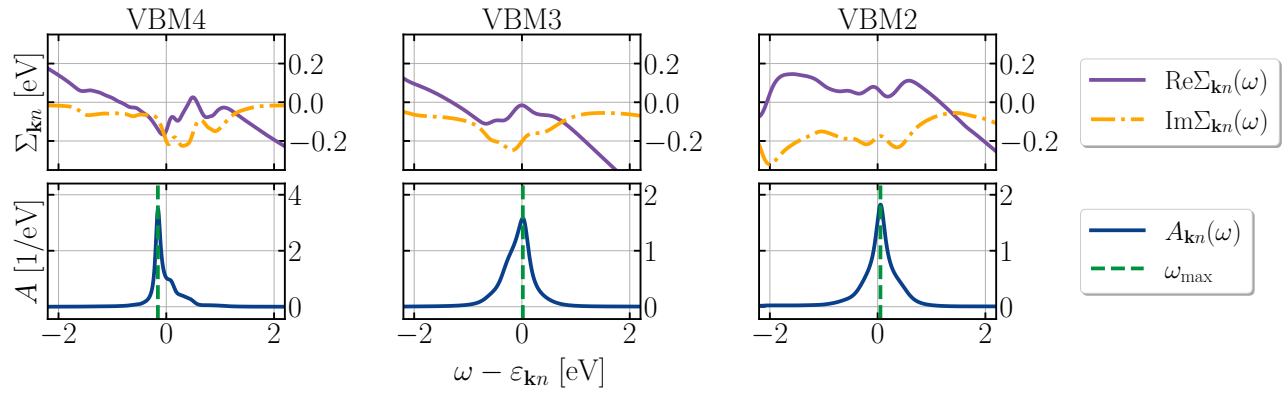

Fig. S15. The frequency dependence of the self-energy and the spectral function for bands VBM4, VBM3, and VBM2 at the R point in the case of $CsPbI_3$ material at $T = 400$ K.

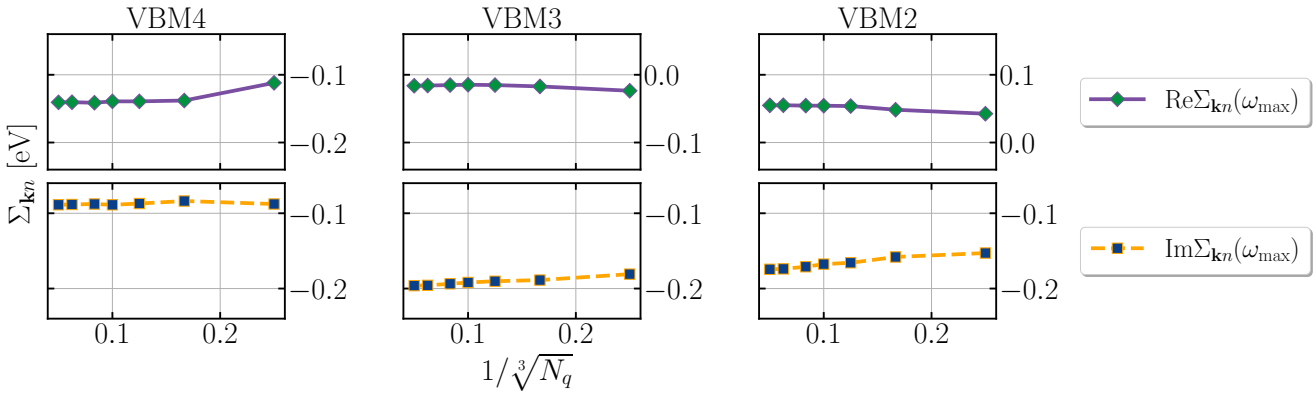

Fig. S16. The dependence of the real and imaginary part of self-energy at the renormalized energy on the size of the q-points grid. The results are presented for $CsPbI_3$ material at $T = 400$ K for bands VBM4, VBM3, and VBM2 at the R point.

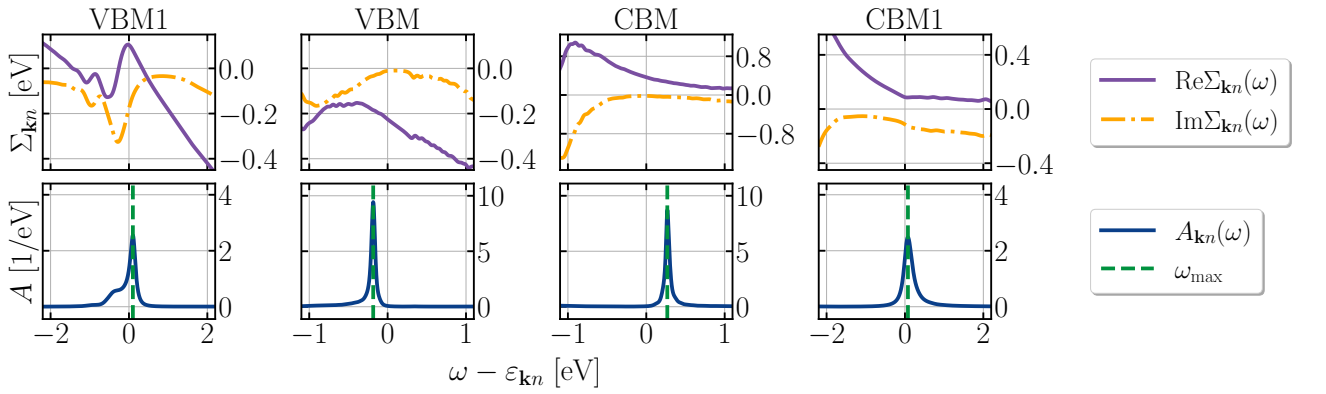

Fig. S17. The frequency dependence of the self-energy and the spectral function for bands VBM1, VBM, CBM and CBM1 at the R point in the case of $CsPbI_3$ material at $T = 400$ K.

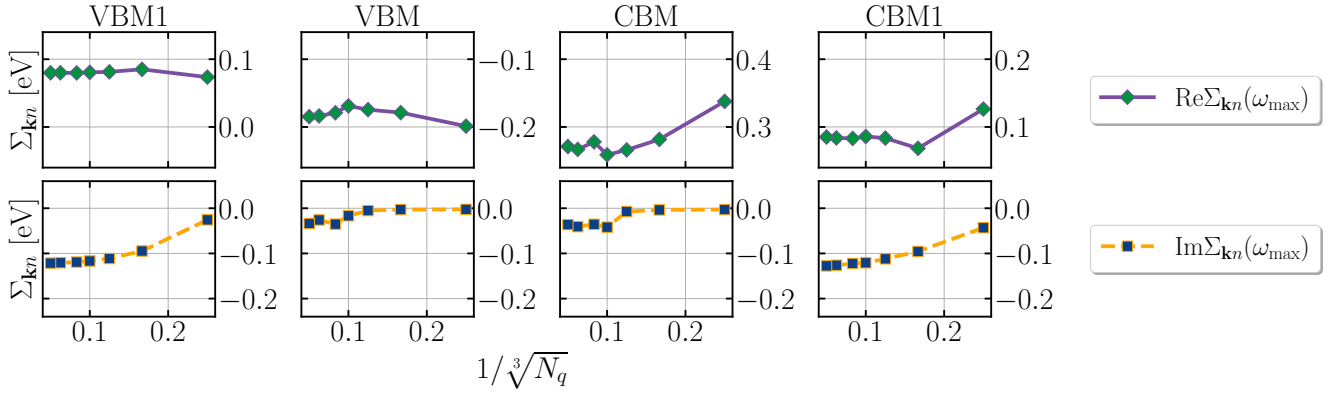

Fig. S18. The dependence of the real and imaginary part of self-energy at the renormalized energy on the size of the q-points grid. The results are presented for $CsPbI_3$ material at $T = 400$ K for bands VBM1, VBM, CBM and CBM1 at the R point.

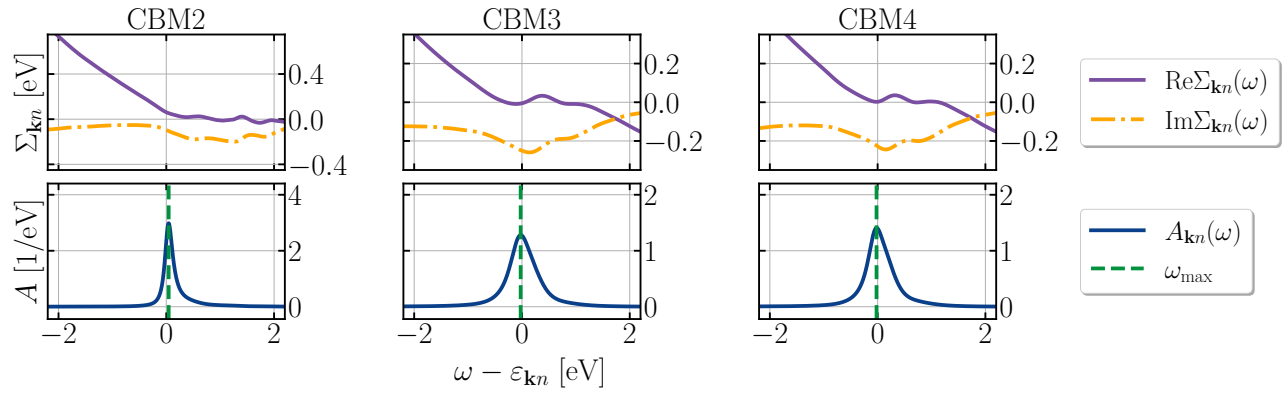

Fig. S19. The frequency dependence of the self-energy and the spectral function for bands CBM2, CBM3, and CBM4 at the R point in the case of $CsPbI_3$ material at $T = 400$ K.

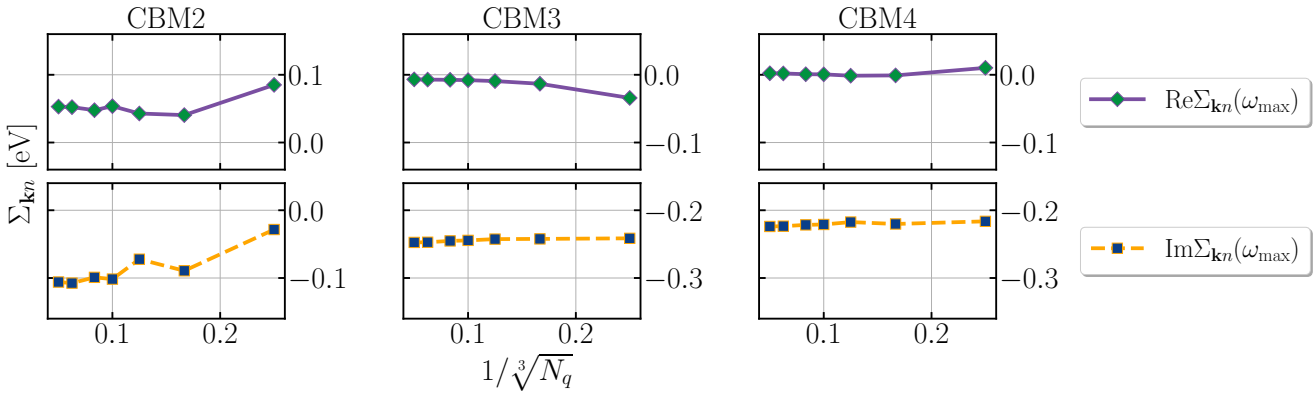

Fig. S20. The dependence of the real and imaginary part of self-energy at the renormalized energy on the size of the q-points grid. The results are presented for $CsPbI_3$ material at $T = 400$ K for bands CBM2, CBM3, and CBM4 at the R point.

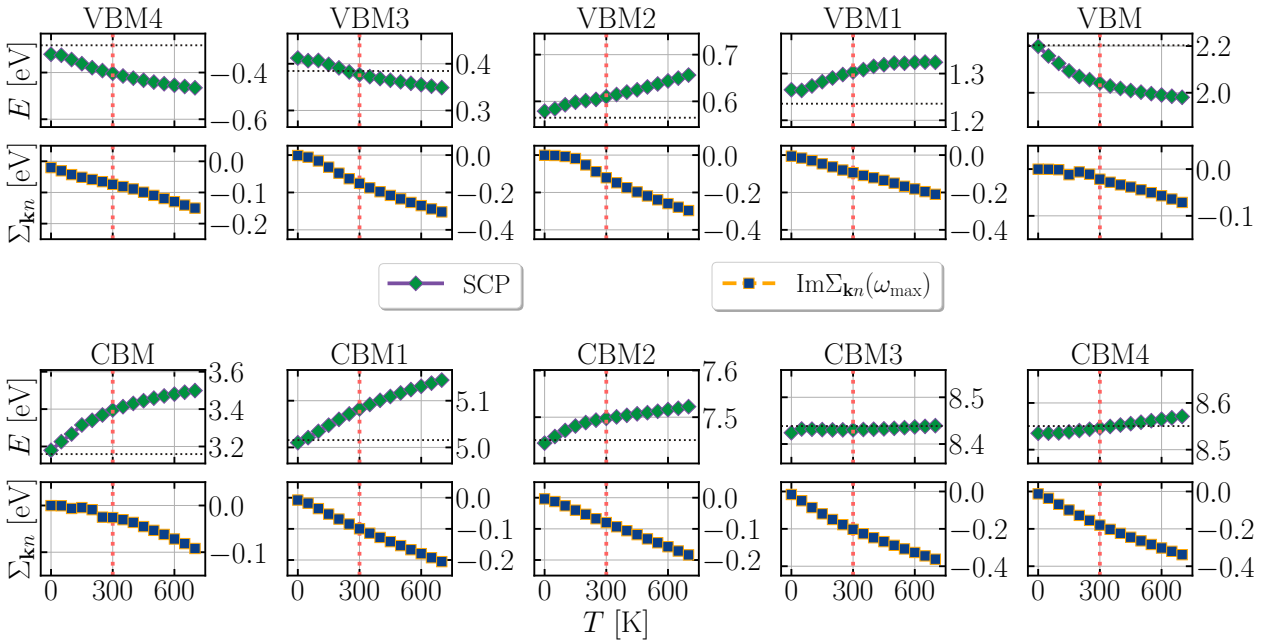

Fig. S21. Temperature dependence of the band energy and the imaginary part of the self-energy for VBM and VBMx (CBM and CBMx) bands (where $x = 1, 2, 3, 4$) calculated using the SCP approach. The results are shown for $CsPbI_3$ at the R point. Vertical and horizontal dotted lines represent the temperature of the phase transition to cubic structure $T_c = 300$ K and band energy from PBE0 calculations, respectively.

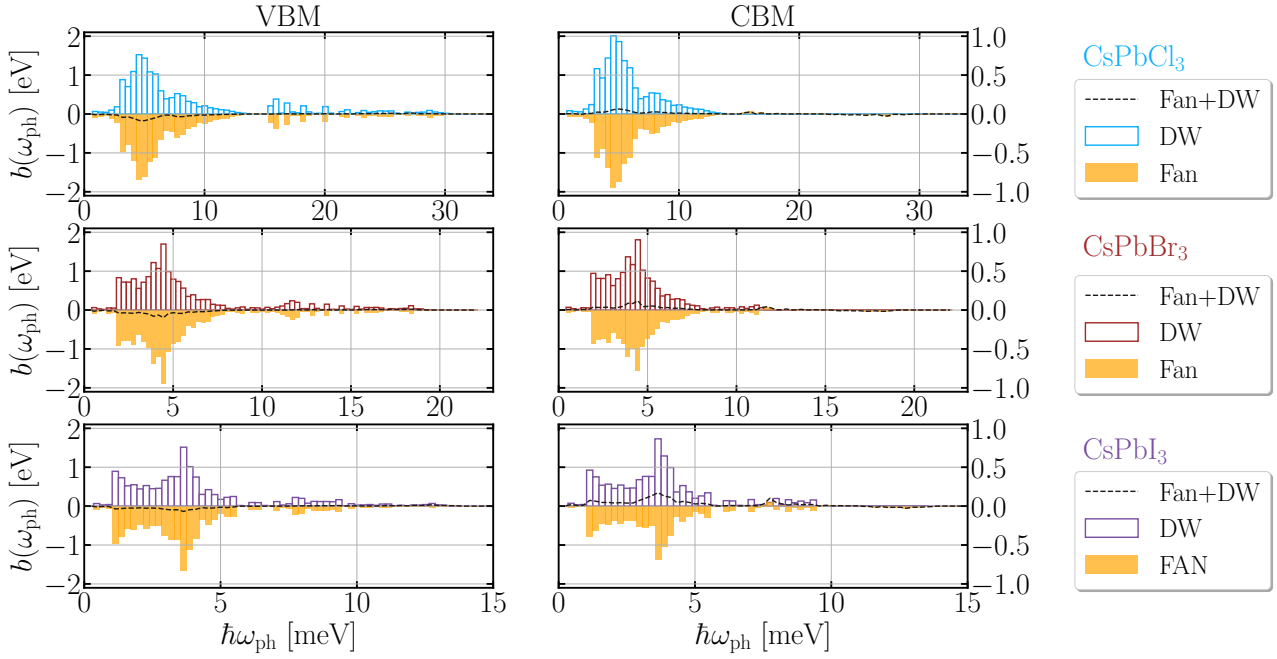

Fig. S22. Contributions from Fan and Debye-Waller terms of phonons at different frequencies to VBM (left column) and CBM (right column) renormalization at $T = 400$ K for $CsPbX_3$ (X = Cl, Br or I, in rows from top to bottom) obtained using the OTMS approach. The value of each bin $b(\omega_i)$ represents the contribution of all phonons with frequencies from the range $(\omega_i - \Delta\omega/2, \omega_i + \Delta\omega/2)$ to band energy renormalization, so that $\Delta E_{\mathbf{k}n} = \sum_i b(\omega_i)$.

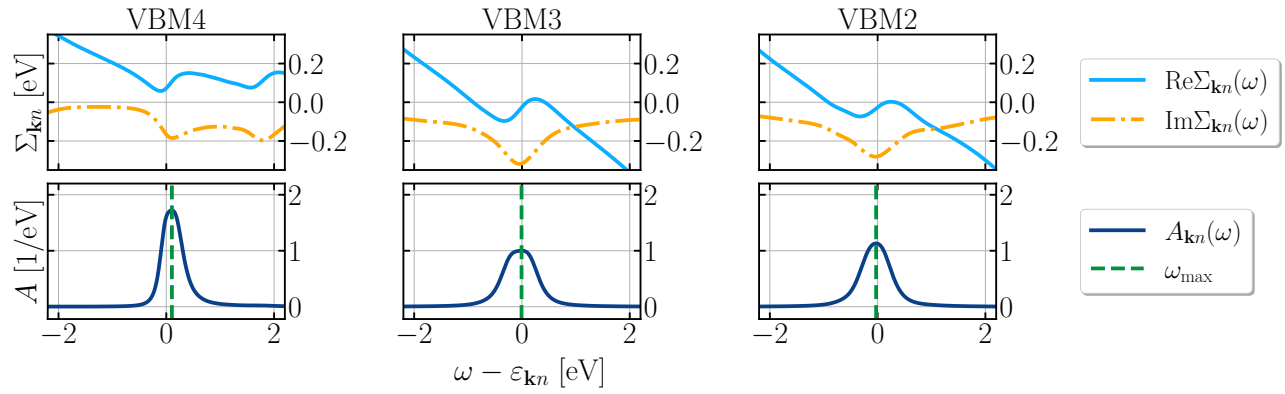

Fig. S23. The frequency dependence of the self-energy and the spectral function for bands VBM4, VBM3, and VBM2 at the Γ point in the case of $CsPbCl_3$ material at $T = 400$ K.

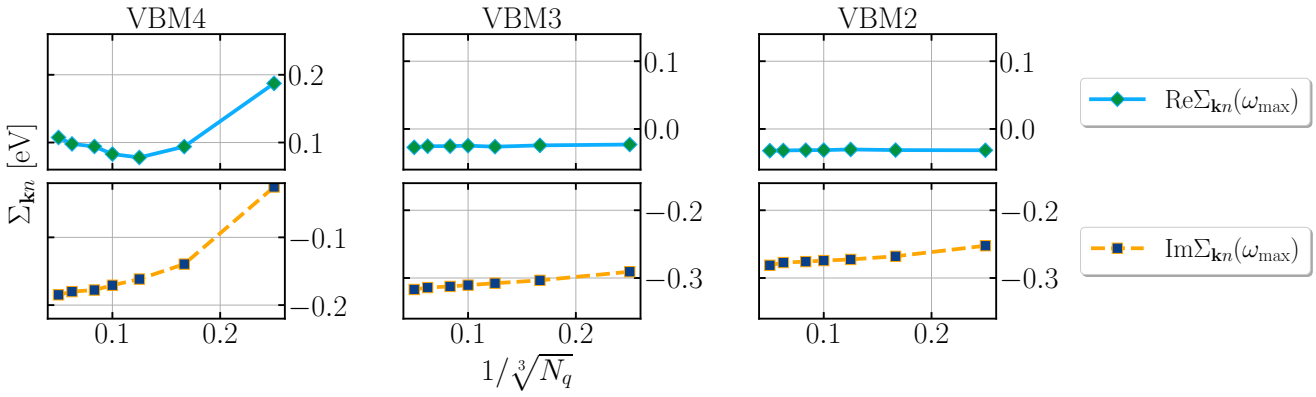

Fig. S24. The dependence of the real and imaginary part of self-energy at the renormalized energy on the size of the q-points grid. The results are presented for $CsPbCl_3$ material at $T = 400$ K for bands VBM4, VBM3, and VBM2 at the Γ point.

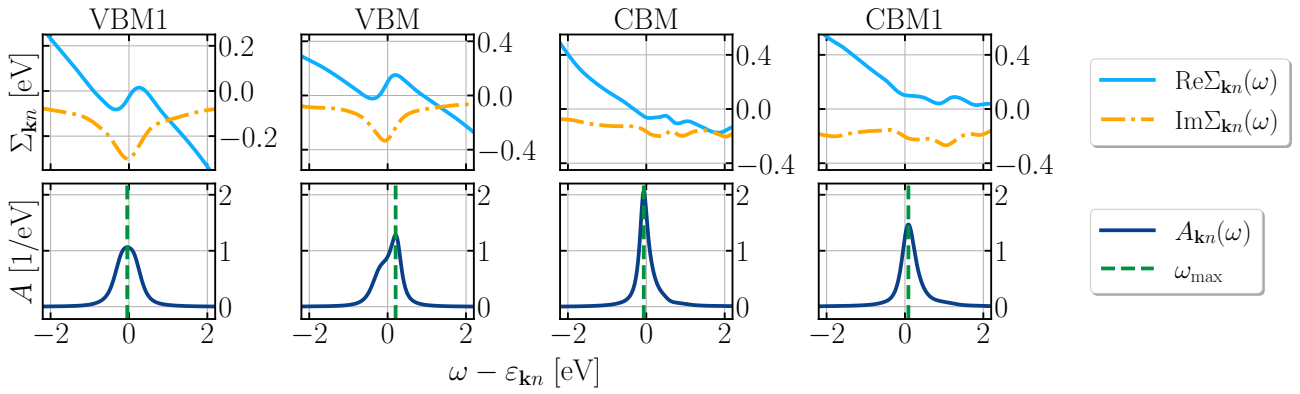

Fig. S25. The frequency dependence of the self-energy and the spectral function for bands VBM1, VBM, CBM and CBM1 at the Γ point in the case of $CsPbCl_3$ material at $T = 400$ K.

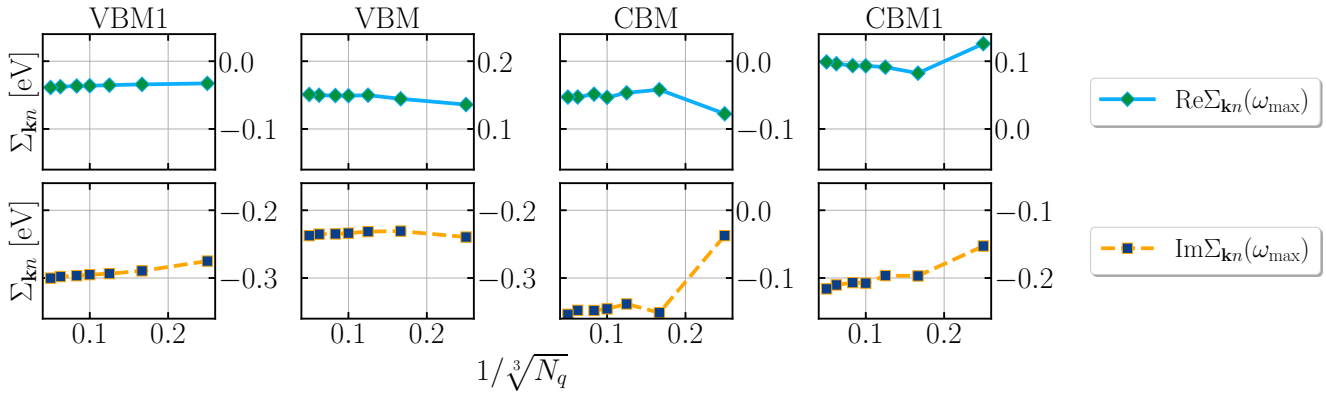

Fig. S26. The dependence of the real and imaginary part of self-energy at the renormalized energy on the size of the q-points grid. The results are presented for $CsPbCl_3$ material at $T = 400$ K for bands VBM1, VBM, CBM and CBM1 at the Γ point.

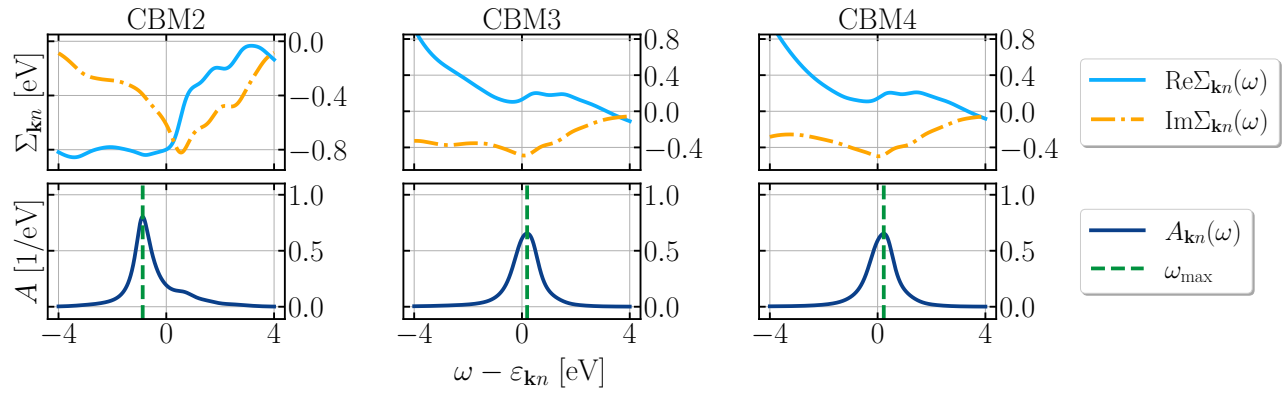

Fig. S27. The frequency dependence of the self-energy and the spectral function for bands CBM2, CBM3, and CBM4 at the Γ point in the case of $CsPbCl_3$ material at $T = 400$ K.

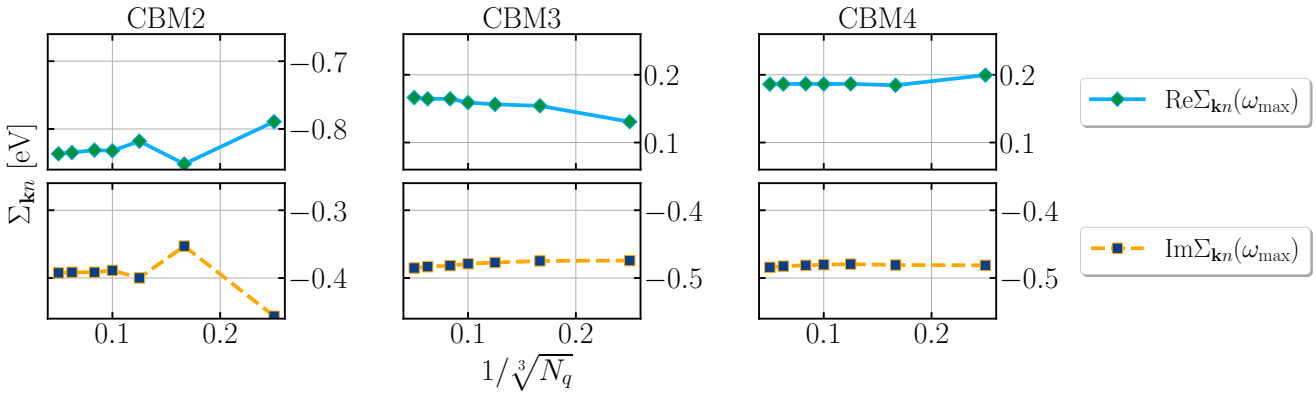

Fig. S28. The dependence of the real and imaginary part of self-energy at the renormalized energy on the size of the q-points grid. The results are presented for $CsPbCl_3$ material at $T = 400$ K for bands CBM2, CBM3, and CBM4 at the Γ point.

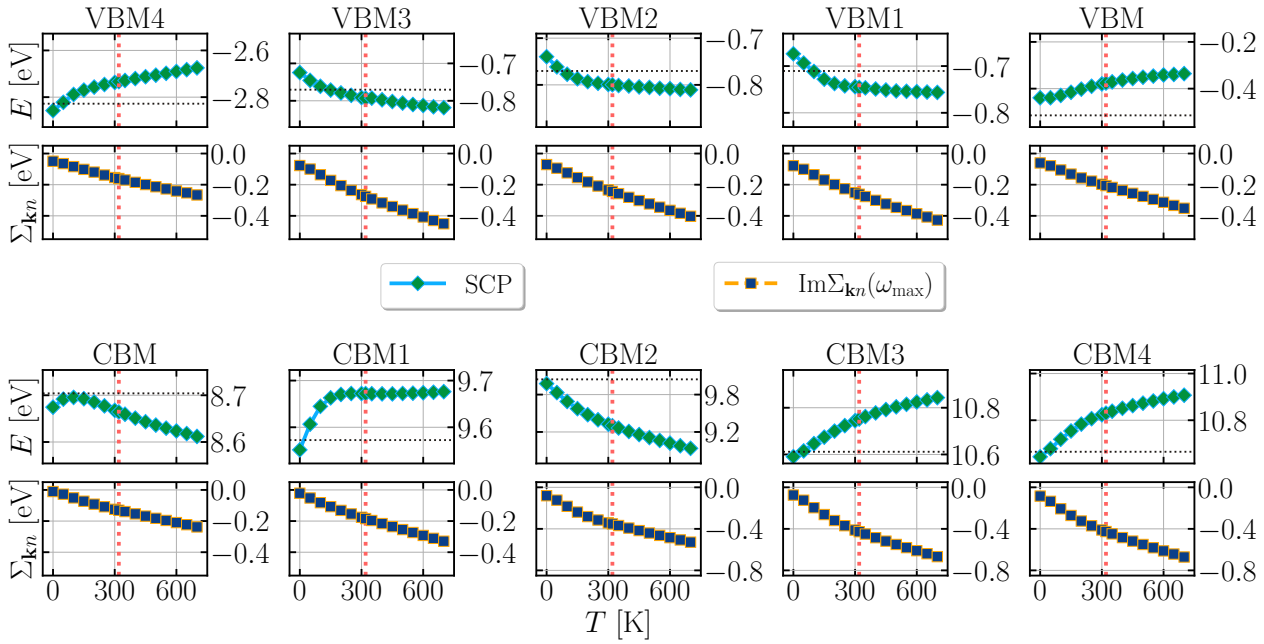

Fig. S29. Temperature dependence of the band energy and the imaginary part of the self-energy for VBM and VBMx (CBM and CBMx) bands (where $x = 1, 2, 3, 4$) calculated using the SCP approach. The results are shown for $CsPbCl_3$ at the Γ point. Vertical and horizontal dotted lines represent the temperature of the phase transition to cubic structure $T_c = 320$ K and band energy from PBE0 calculations, respectively.

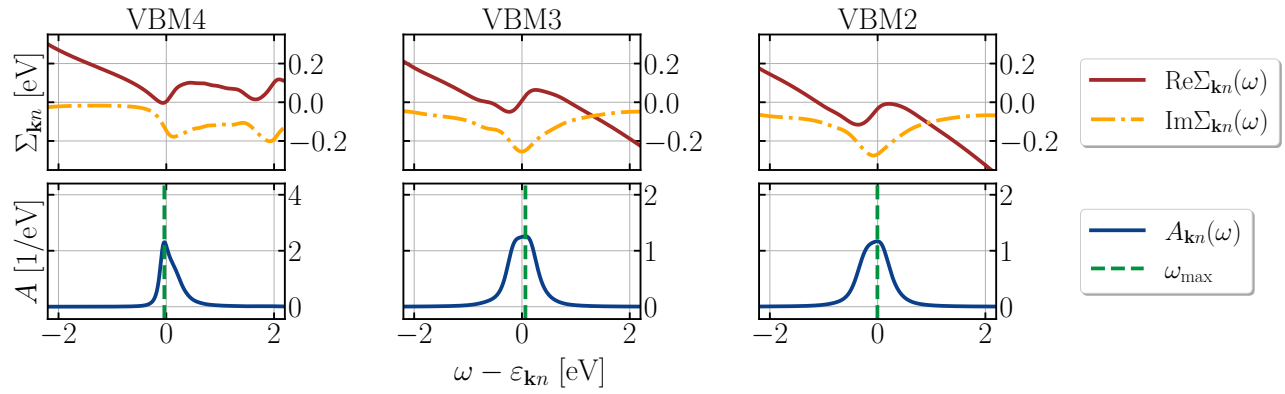

Fig. S30. The frequency dependence of the self-energy and the spectral function for bands VBM4, VBM3, and VBM2 at the Γ point in the case of $CsPbBr_3$ material at $T = 400$ K.

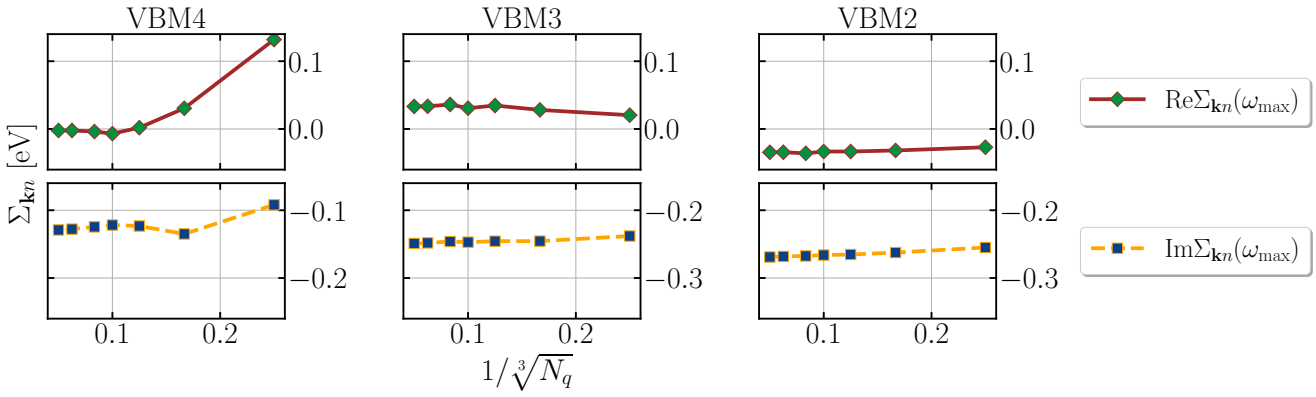

Fig. S31. The dependence of the real and imaginary part of self-energy at the renormalized energy on the size of the q-points grid. The results are presented for $CsPbBr_3$ material at $T = 400$ K for bands VBM4, VBM3, and VBM2 at the Γ point.

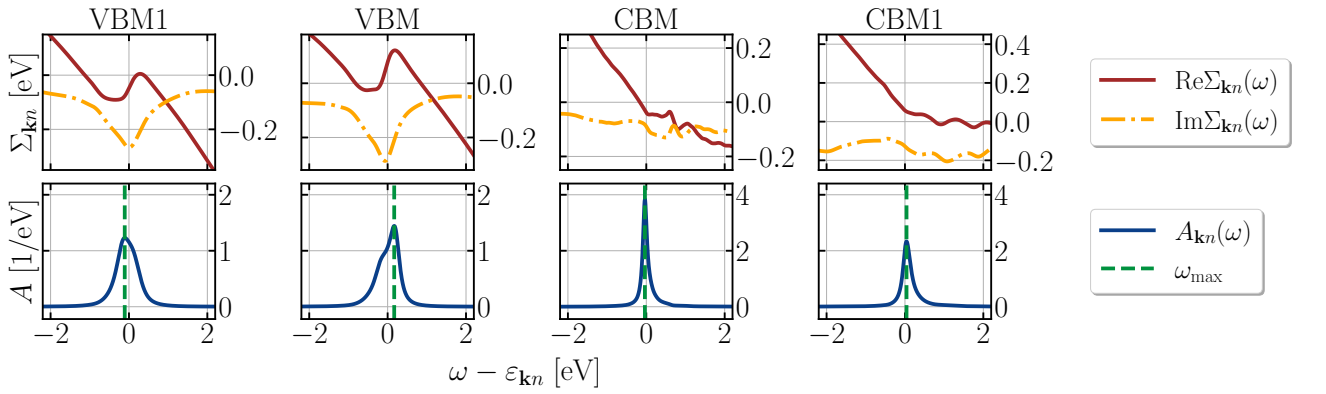

Fig. S32. The frequency dependence of the self-energy and the spectral function for bands VBM1, VBM, CBM and CBM1 at the Γ point in the case of $CsPbBr_3$ material at $T = 400$ K.

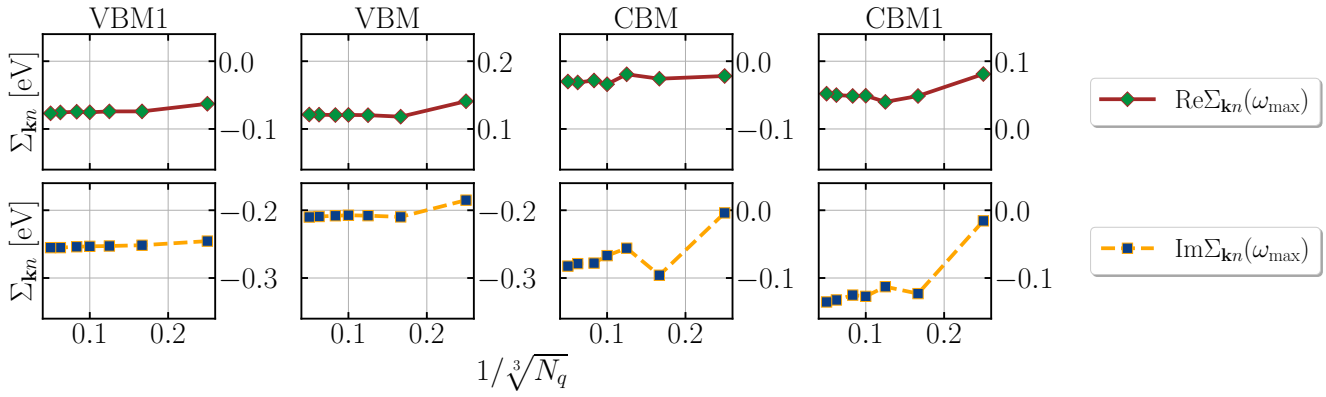

Fig. S33. The dependence of the real and imaginary part of self-energy at the renormalized energy on the size of the q-points grid. The results are presented for $CsPbBr_3$ material at $T = 400$ K for bands VBM1, VBM, CBM and CBM1 at the Γ point.

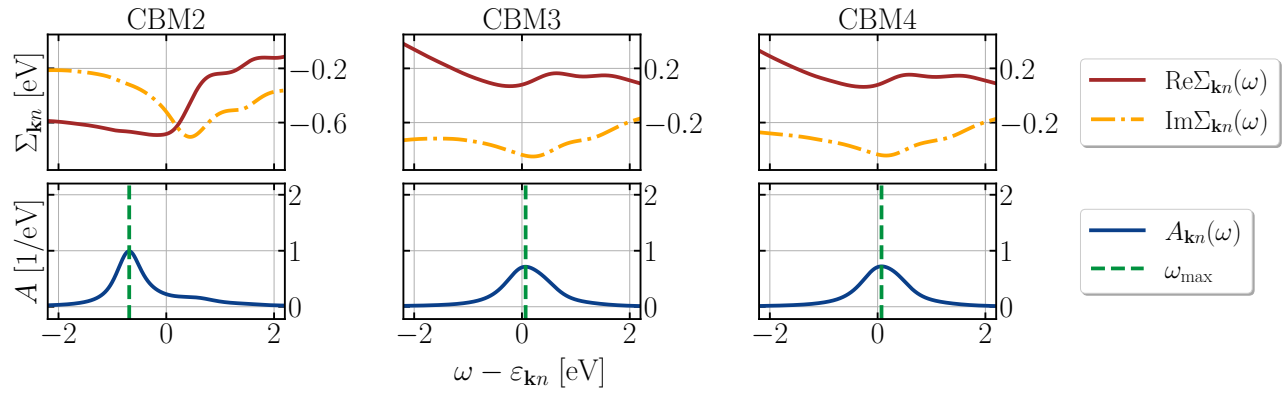

Fig. S34. The frequency dependence of the self-energy and the spectral function for bands CBM2, CBM3, and CBM4 at the Γ point in the case of $CsPbBr_3$ material at $T = 400$ K.

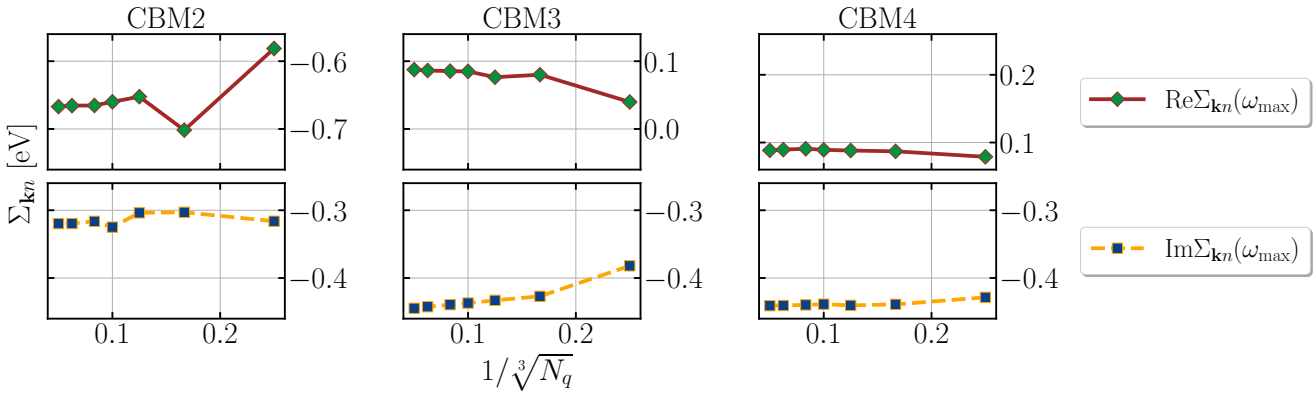

Fig. S35. The dependence of the real and imaginary part of self-energy at the renormalized energy on the size of the q-points grid. The results are presented for $CsPbBr_3$ material at $T = 400$ K for bands CBM2, CBM3, and CBM4 at the Γ point.

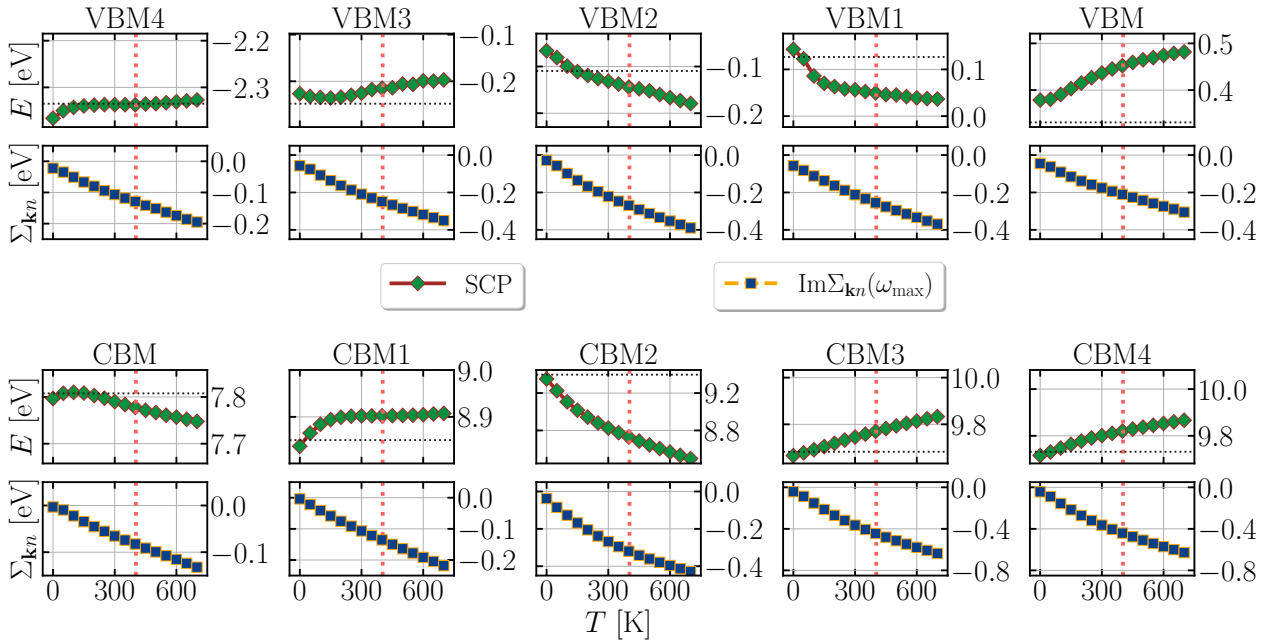

Fig. S36. Temperature dependence of the band energy and the imaginary part of the self-energy for VBM and VBMx (CBM and CBMx) bands (where $x = 1, 2, 3, 4$) calculated using the SCP approach. The results are shown for $CsPbBr_3$ at the Γ point. Vertical and horizontal dotted lines represent the temperature of the phase transition to cubic structure $T_c = 403\,\mathrm{K}$ and band energy from PBE0 calculations, respectively.

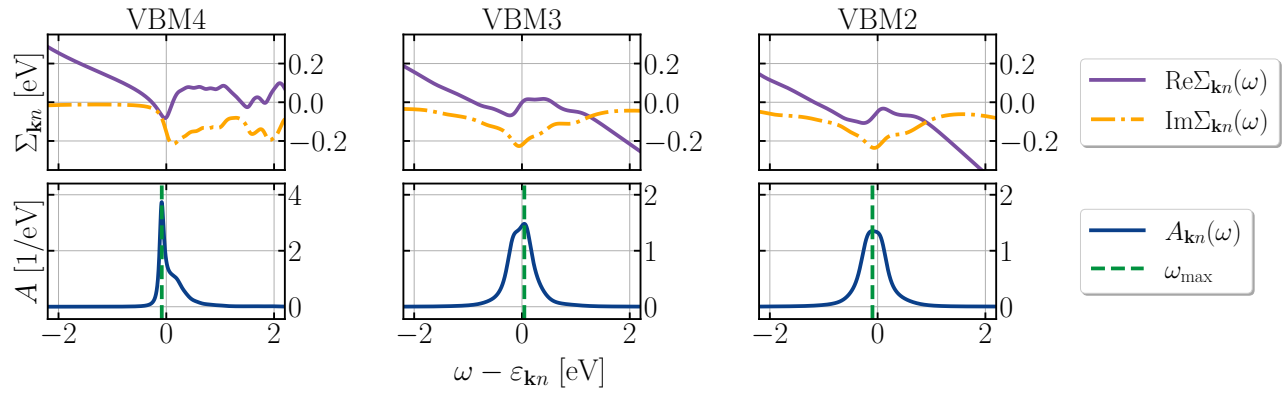

Fig. S37. The frequency dependence of the self-energy and the spectral function for bands VBM4, VBM3, and VBM2 at the Γ point in the case of $CsPbI_3$ material at $T = 400$ K.

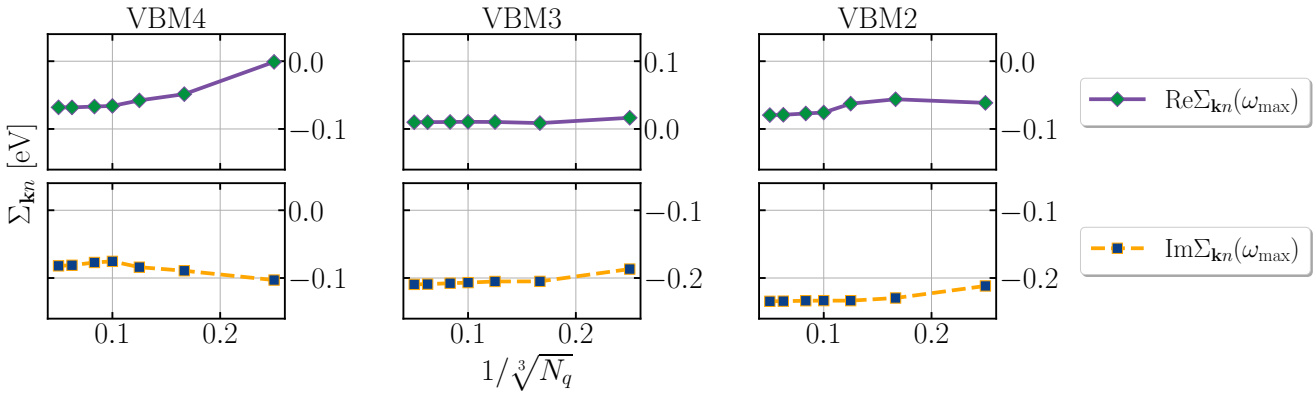

Fig. S38. The dependence of the real and imaginary part of self-energy at the renormalized energy on the size of the q-points grid. The results are presented for $CsPbI_3$ material at $T = 400$ K for bands VBM4, VBM3, and VBM2 at the Γ point.

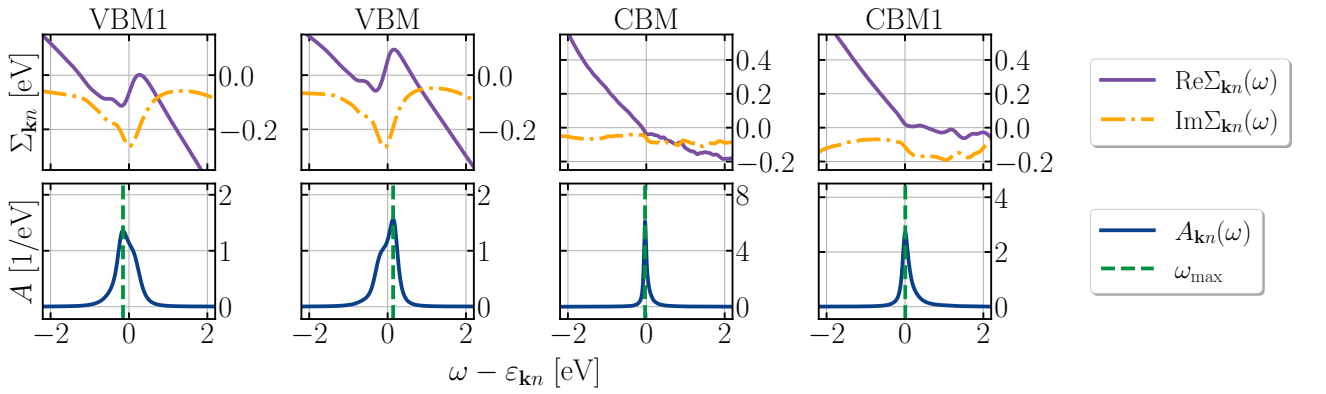

Fig. S39. The frequency dependence of the self-energy and the spectral function for bands VBM1, VBM, CBM and CBM1 at the Γ point in the case of $CsPbI_3$ material at $T = 400$ K.

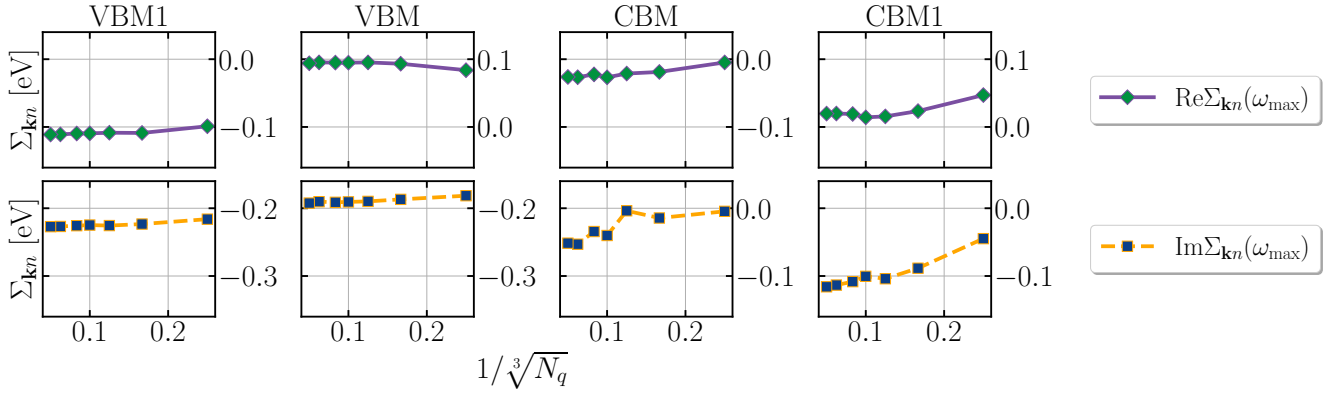

Fig. S40. The dependence of the real and imaginary part of self-energy at the renormalized energy on the size of the q-points grid. The results are presented for $CsPbI_3$ material at $T = 400$ K for bands VBM1, VBM, CBM and CBM1 at the Γ point.

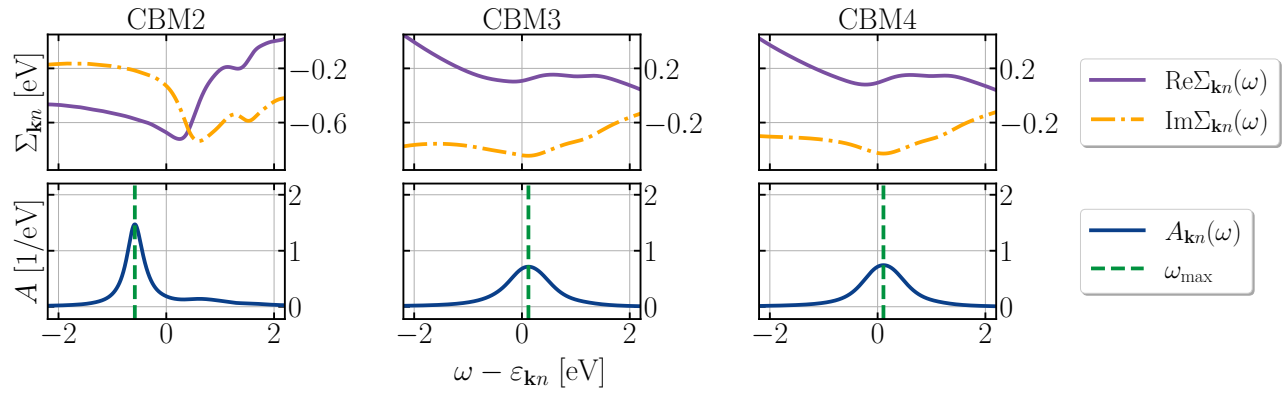

Fig. S41. The frequency dependence of the self-energy and the spectral function for bands CBM2, CBM3, and CBM4 at the Γ point in the case of $CsPbI_3$ material at $T = 400$ K.

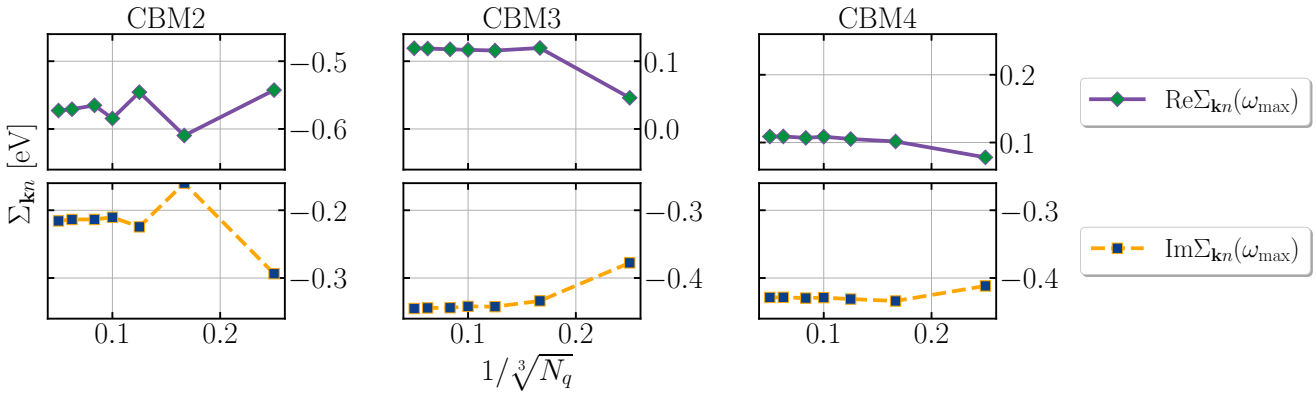

Fig. S42. The dependence of the real and imaginary part of self-energy at the renormalized energy on the size of the q-points grid. The results are presented for $CsPbI_3$ material at $T = 400$ K for bands CBM2, CBM3, and CBM4 at the Γ point.

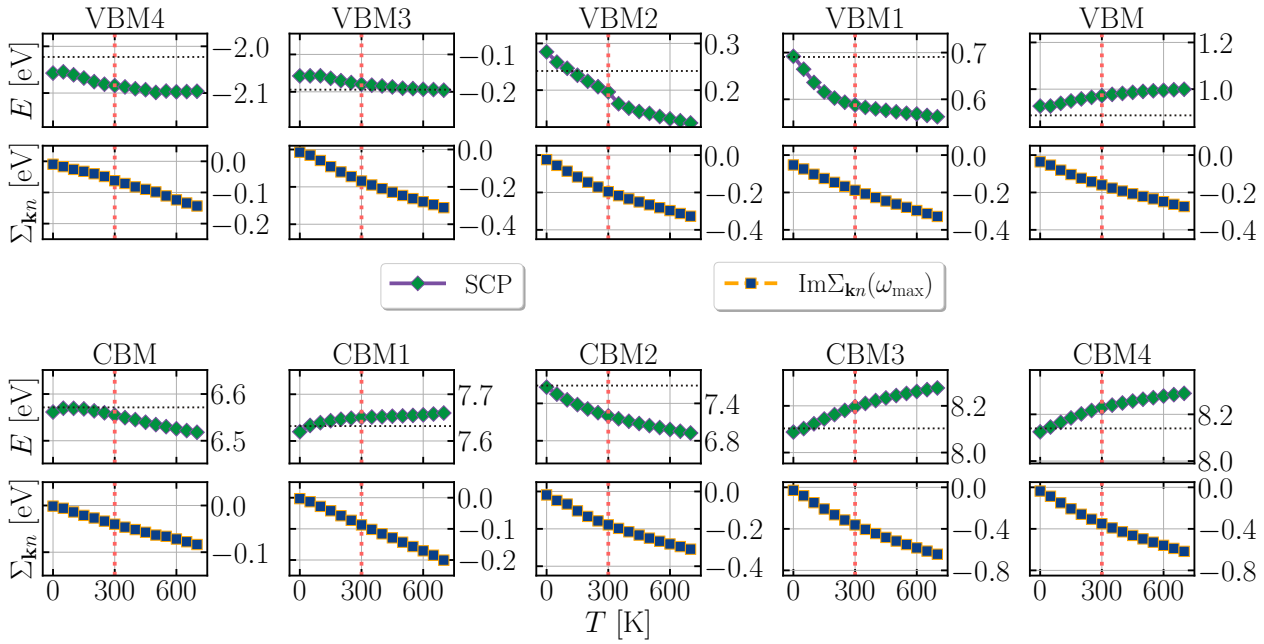

Fig. S43. Temperature dependence of the band energy and the imaginary part of the self-energy for VBM and VBMx (CBM and CBMx) bands (where $x = 1, 2, 3, 4$) calculated using the SCP approach. The results are shown for $CsPbI_3$ at the Γ point. Vertical and horizontal dotted lines represent the temperature of the phase transition to cubic structure $T_c = 300$ K and band energy from PBE0 calculations, respectively.

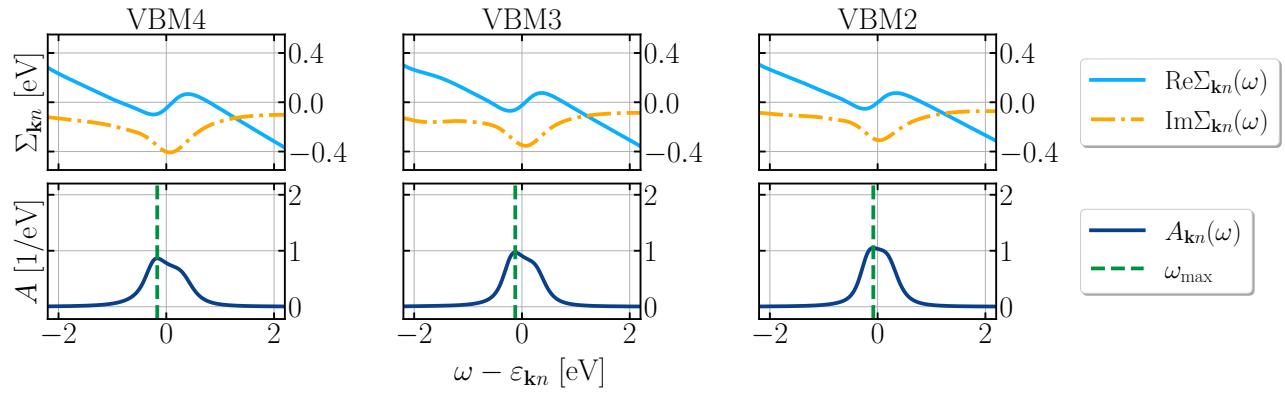

Fig. S44. The frequency dependence of the self-energy and the spectral function for bands VBM4, VBM3, and VBM2 at the X point in the case of $CsPbCl_3$ material at $T = 400$ K.

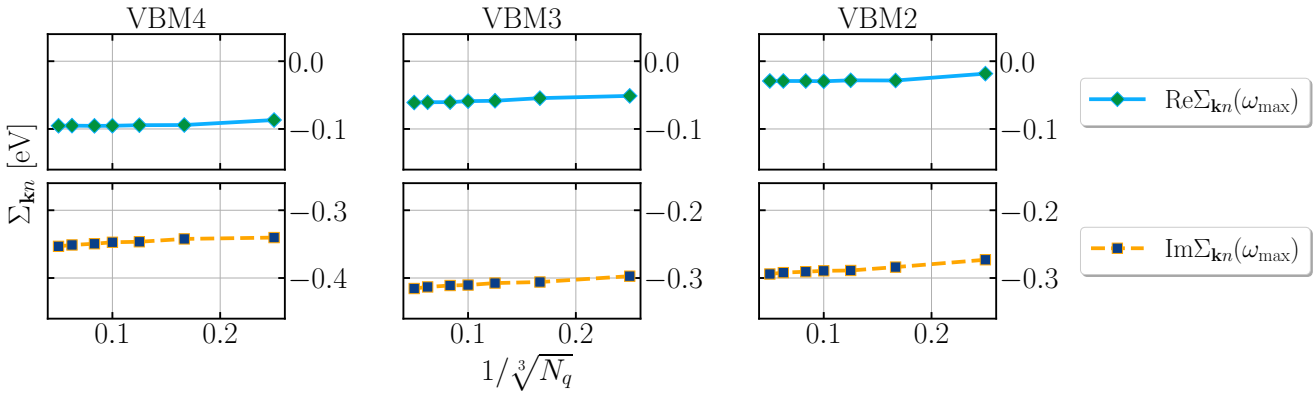

Fig. S45. The dependence of the real and imaginary part of self-energy at the renormalized energy on the size of the q-points grid. The results are presented for $CsPbCl_3$ material at $T = 400$ K for bands VBM4, VBM3, and VBM2 at the X point.

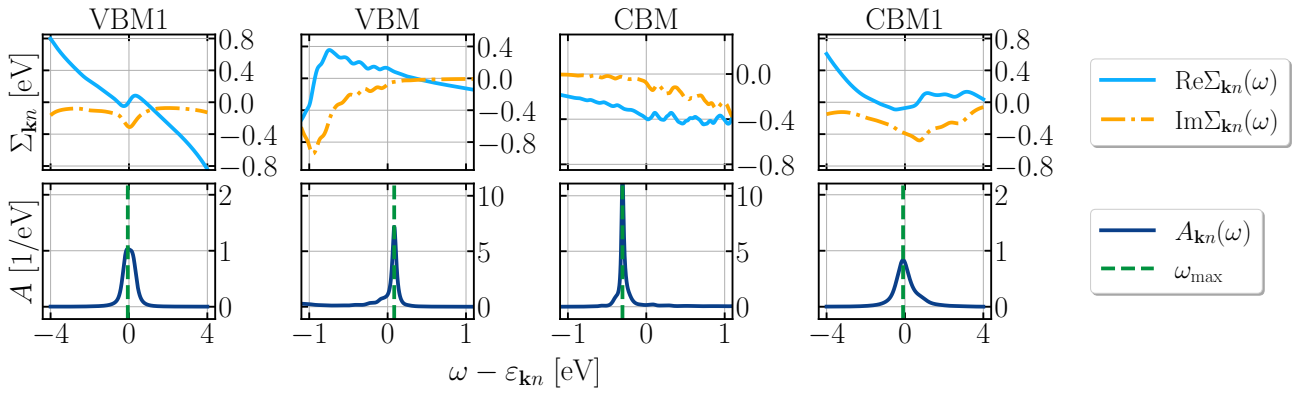

Fig. S46. The frequency dependence of the self-energy and the spectral function for bands VBM1, VBM, CBM and CBM1 at the X point in the case of $CsPbCl_3$ material at $T = 400$ K.

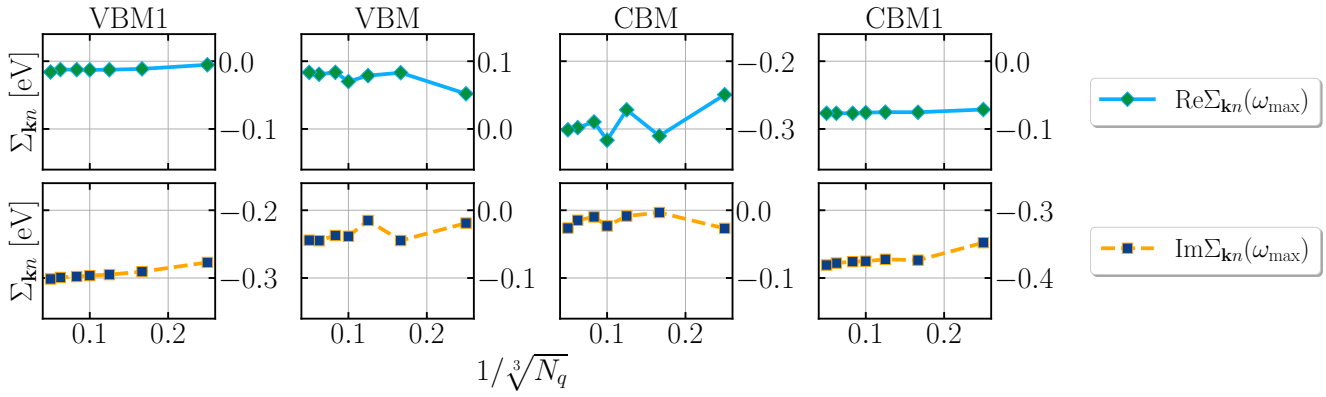

Fig. S47. The dependence of the real and imaginary part of self-energy at the renormalized energy on the size of the q-points grid. The results are presented for $CsPbCl_3$ material at $T = 400$ K for bands VBM1, VBM, CBM and CBM1 at the X point.

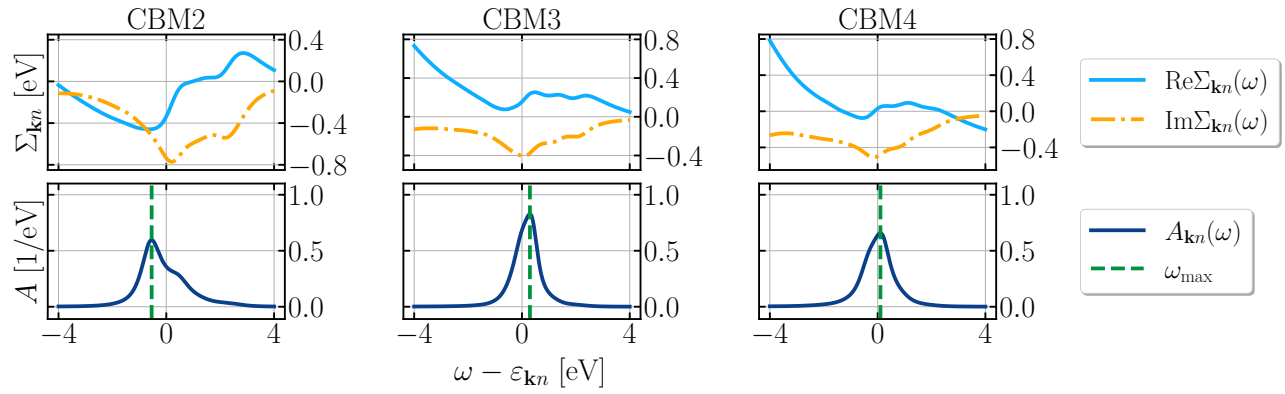

Fig. S48. The frequency dependence of the self-energy and the spectral function for bands CBM2, CBM3, and CBM4 at the X point in the case of $CsPbCl_3$ material at $T = 400$ K.

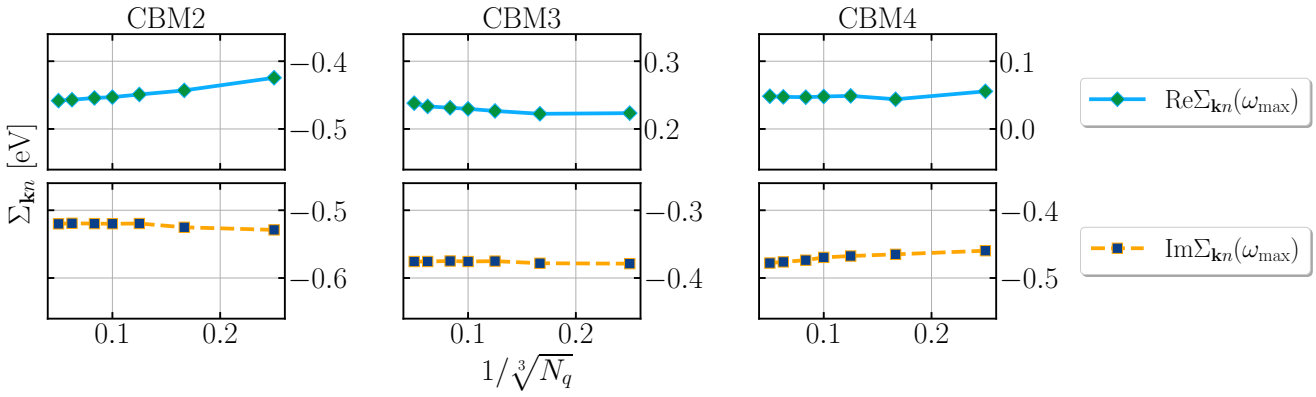

Fig. S49. The dependence of the real and imaginary part of self-energy at the renormalized energy on the size of the q-points grid. The results are presented for $CsPbCl_3$ material at $T = 400$ K for bands CBM2, CBM3, and CBM4 at the X point.

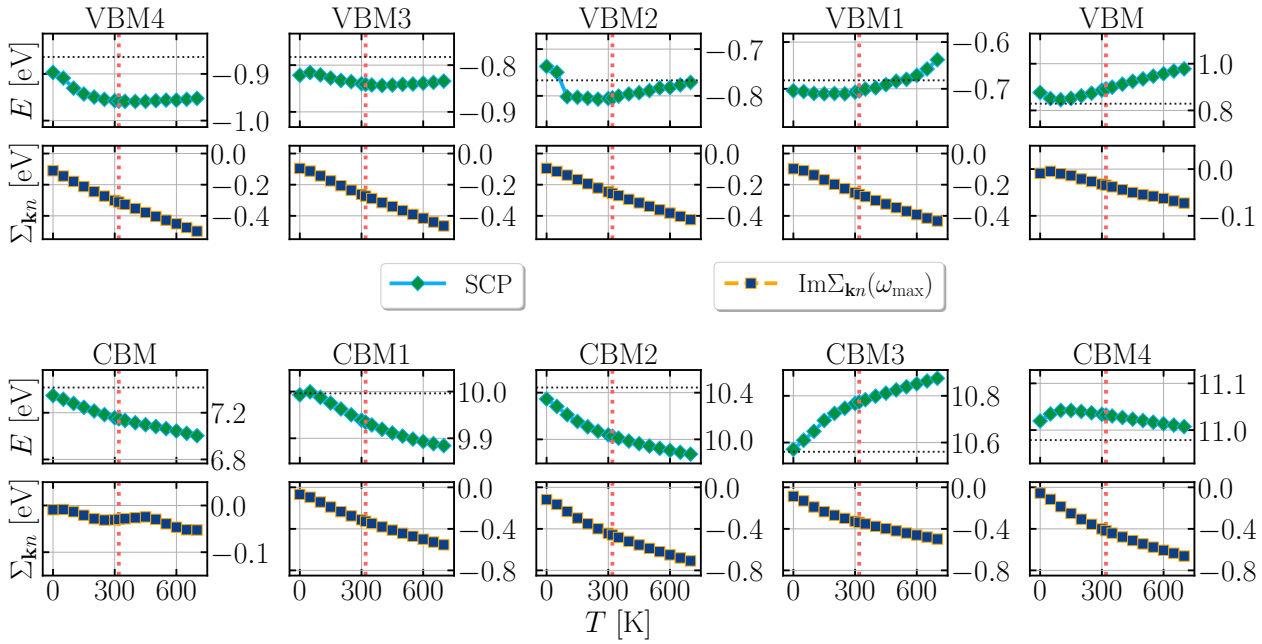

Fig. S50. Temperature dependence of the band energy and the imaginary part of the self-energy for VBM and VBMx (CBM and CBMx) bands (where $x = 1, 2, 3, 4$) calculated using the SCP approach. The results are shown for $CsPbCl_3$ at the X point. Vertical and horizontal dotted lines represent the temperature of the phase transition to cubic structure $T_c = 320$ K and band energy from PBE0 calculations, respectively.

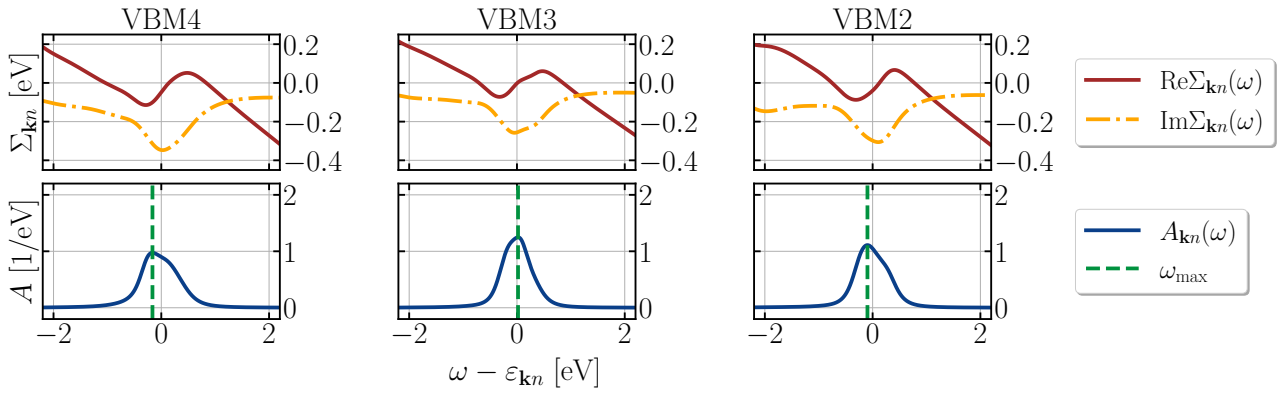

Fig. S51. The frequency dependence of the self-energy and the spectral function for bands VBM4, VBM3, and VBM2 at the X point in the case of $CsPbBr_3$ material at $T = 400$ K.

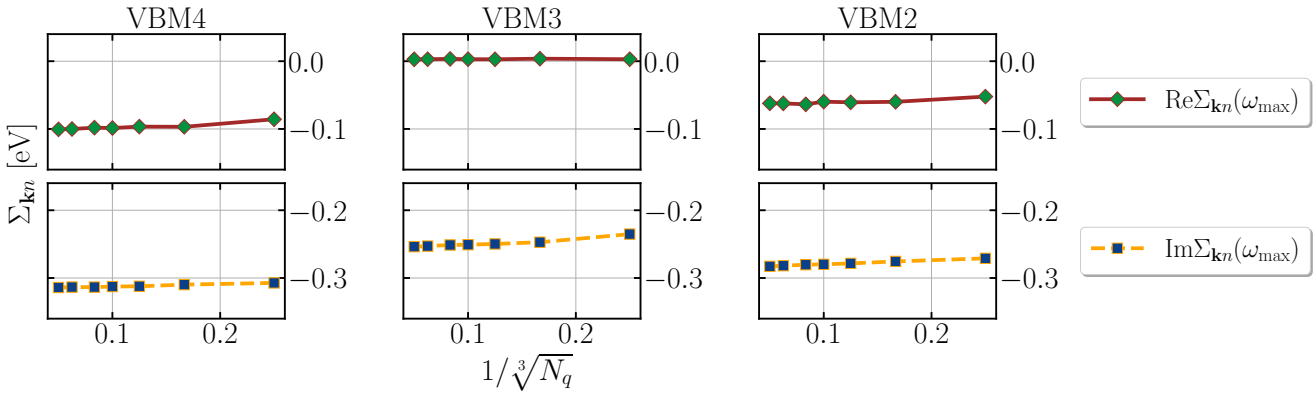

Fig. S52. The dependence of the real and imaginary part of self-energy at the renormalized energy on the size of the q-points grid. The results are presented for $CsPbBr_3$ material at $T = 400$ K for bands VBM4, VBM3, and VBM2 at the X point.

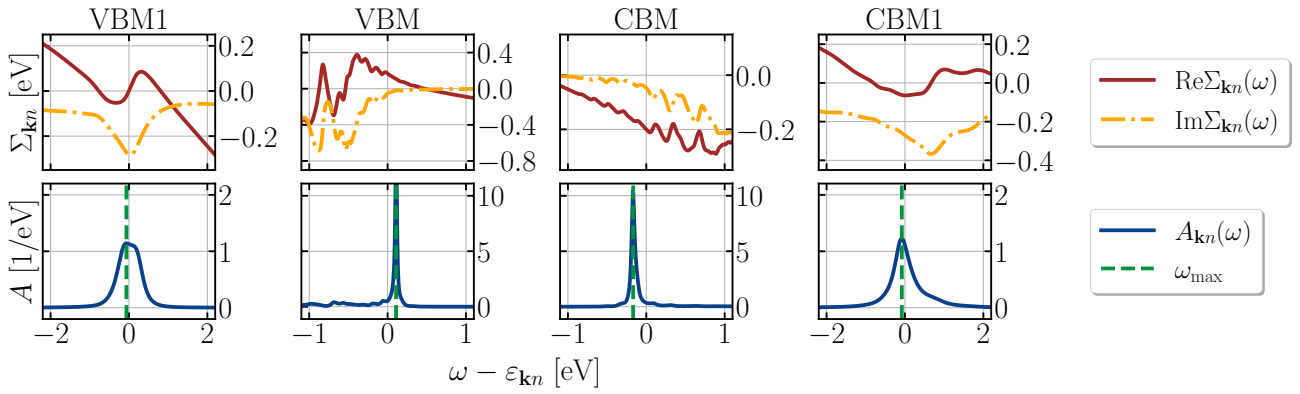

Fig. S53. The frequency dependence of the self-energy and the spectral function for bands VBM1, VBM, CBM and CBM1 at the X point in the case of $CsPbBr_3$ material at $T = 400$ K.

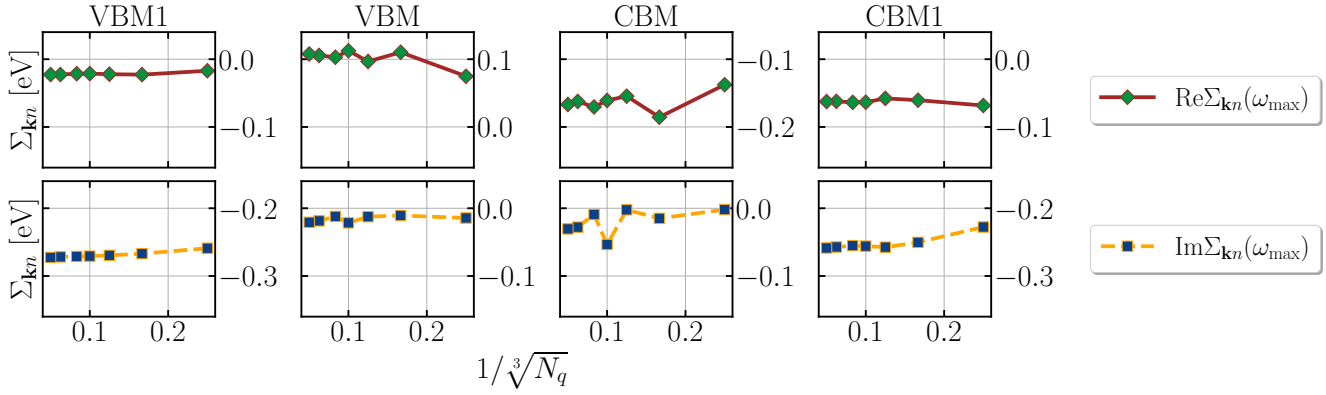

Fig. S54. The dependence of the real and imaginary part of self-energy at the renormalized energy on the size of the q-points grid. The results are presented for $CsPbBr_3$ material at $T = 400$ K for bands VBM1, VBM, CBM and CBM1 at the X point.

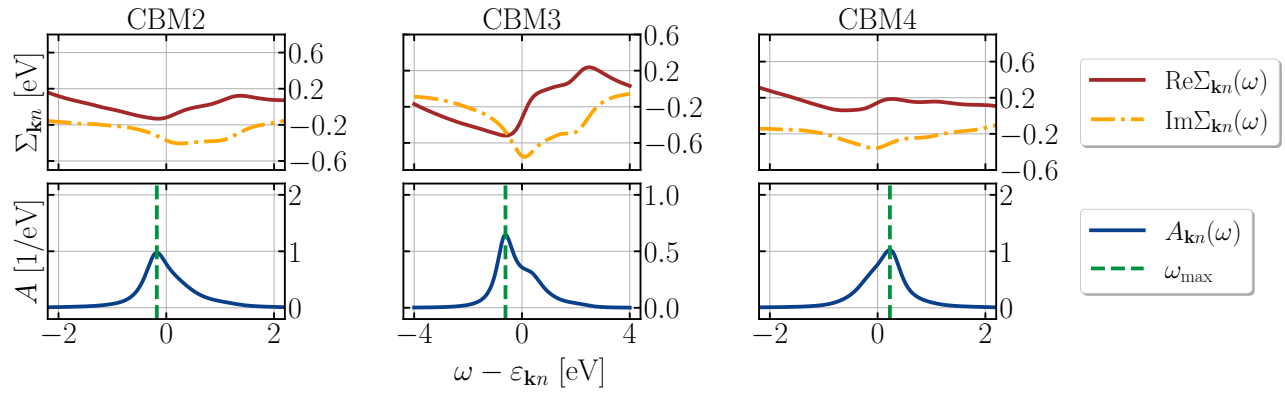

Fig. S55. The frequency dependence of the self-energy and the spectral function for bands CBM2, CBM3, and CBM4 at the X point in the case of $CsPbBr_3$ material at $T = 400$ K.

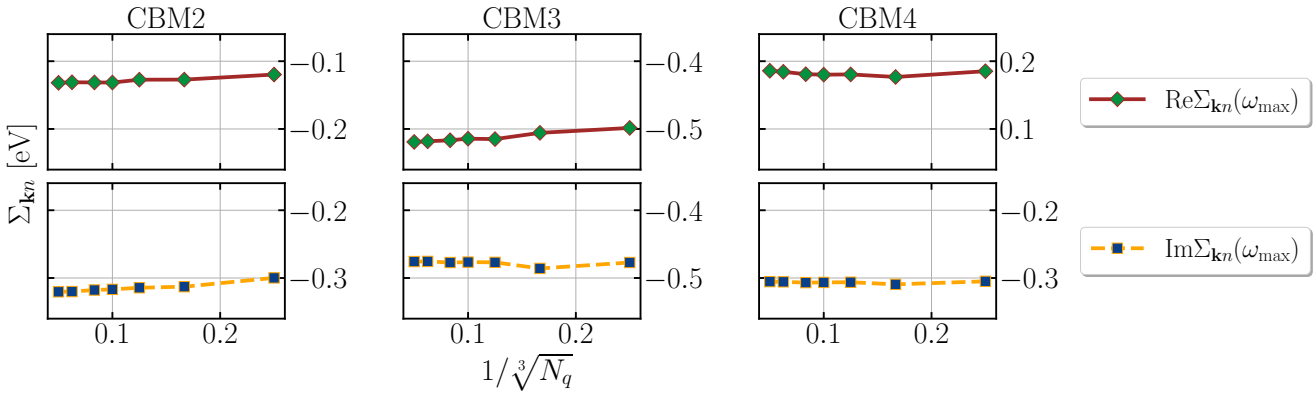

Fig. S56. The dependence of the real and imaginary part of self-energy at the renormalized energy on the size of the q-points grid. The results are presented for $CsPbBr_3$ material at $T = 400$ K for bands CBM2, CBM3, and CBM4 at the X point.

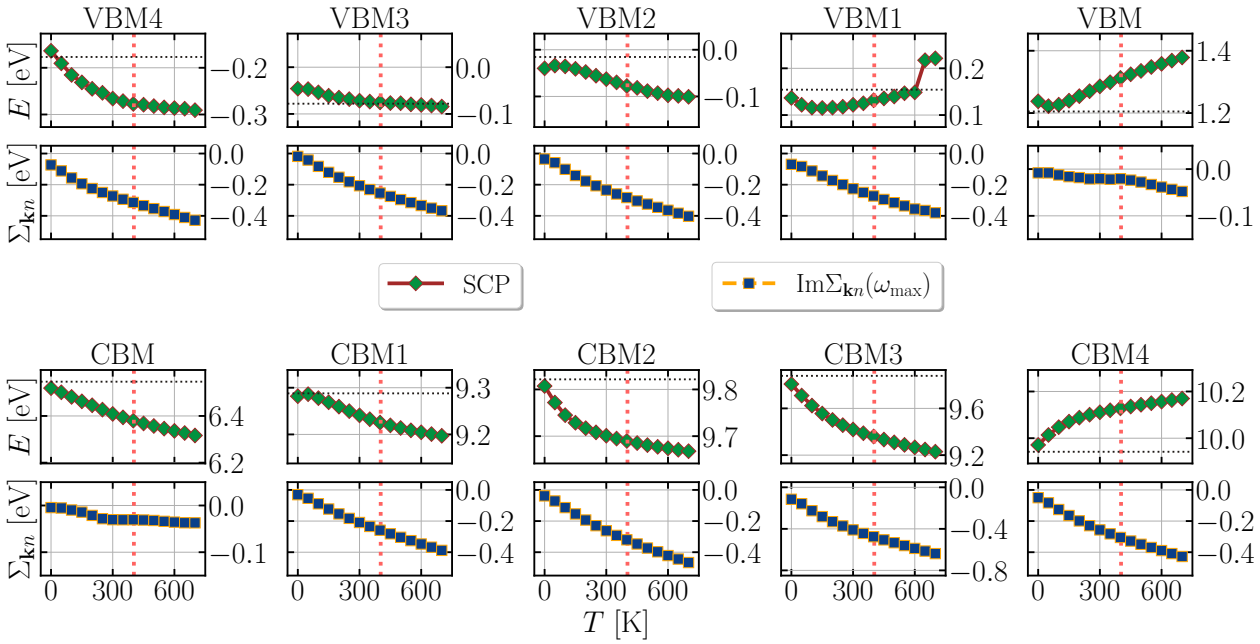

Fig. S57. Temperature dependence of the band energy and the imaginary part of the self-energy for VBM and VBMx (CBM and CBMx) bands (where $x = 1, 2, 3, 4$) calculated using the SCP approach. The results are shown for $CsPbBr_3$ at the X point. Vertical and horizontal dotted lines represent the temperature of the phase transition to cubic structure $T_c = 403\,\mathrm{K}$ and band energy from PBE0 calculations, respectively.

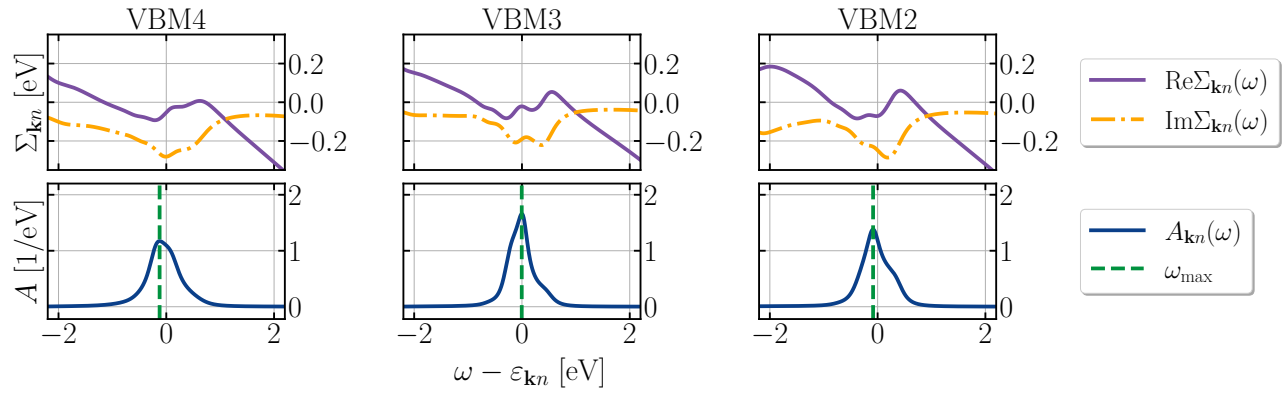

Fig. S58. The frequency dependence of the self-energy and the spectral function for bands VBM4, VBM3, and VBM2 at the X point in the case of $CsPbI_3$ material at $T = 400$ K.

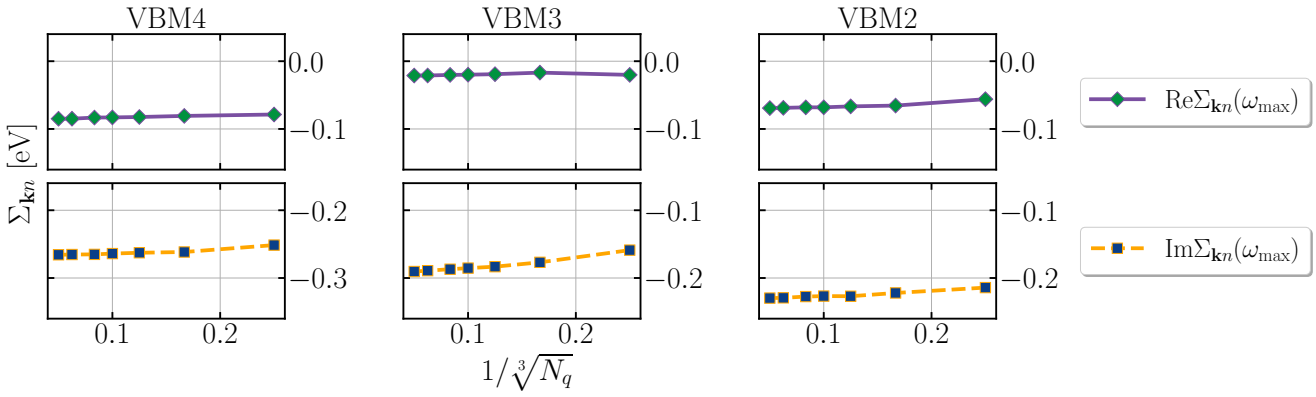

Fig. S59. The dependence of the real and imaginary part of self-energy at the renormalized energy on the size of the q-points grid. The results are presented for $CsPbI_3$ material at $T = 400$ K for bands VBM4, VBM3, and VBM2 at the X point.

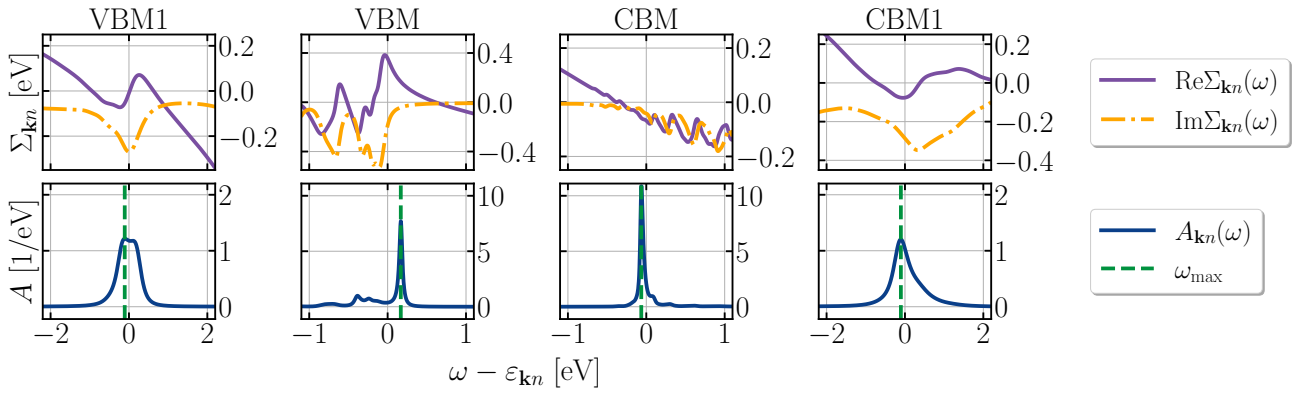

Fig. S60. The frequency dependence of the self-energy and the spectral function for bands VBM1, VBM, CBM and CBM1 at the X point in the case of $CsPbI_3$ material at $T = 400$ K.

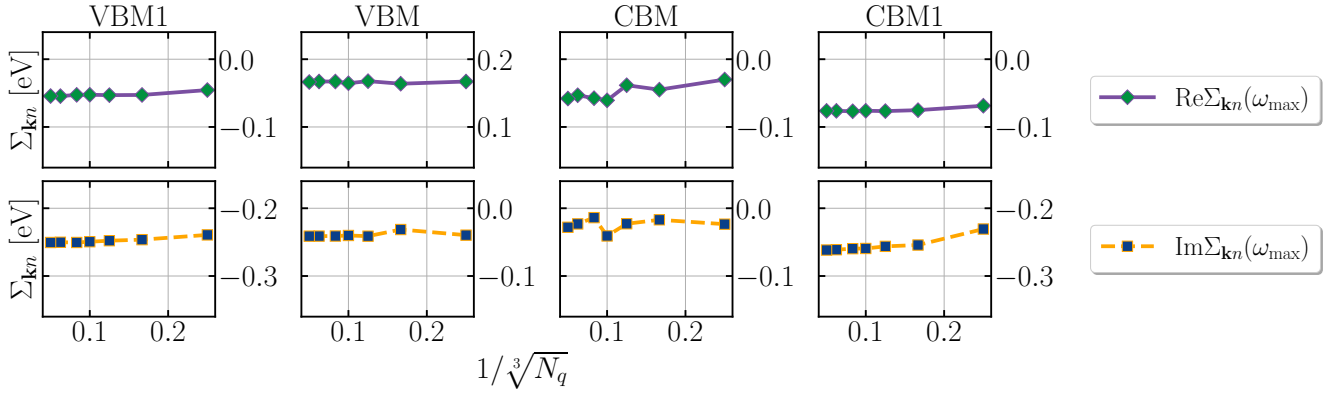

Fig. S61. The dependence of the real and imaginary part of self-energy at the renormalized energy on the size of the q-points grid. The results are presented for $CsPbI_3$ material at $T = 400$ K for bands VBM1, VBM, CBM and CBM1 at the X point.

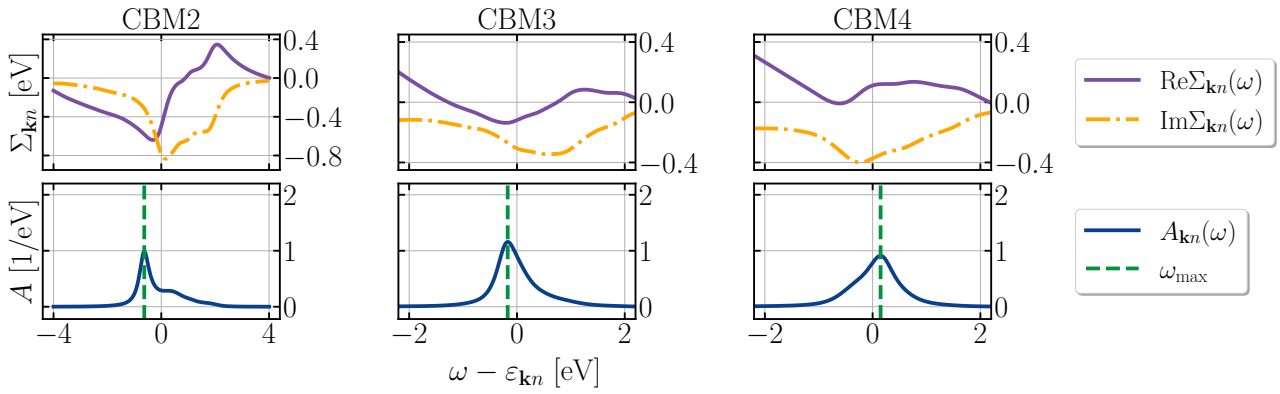

Fig. S62. The frequency dependence of the self-energy and the spectral function for bands CBM2, CBM3, and CBM4 at the X point in the case of $CsPbI_3$ material at $T = 400$ K.

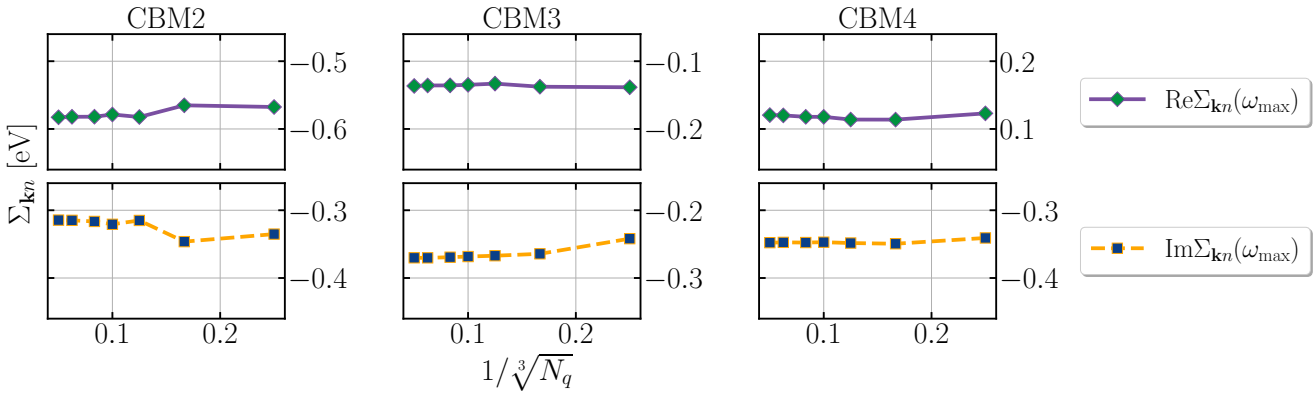

Fig. S63. The dependence of the real and imaginary part of self-energy at the renormalized energy on the size of the q-points grid. The results are presented for $CsPbI_3$ material at $T = 400$ K for bands CBM2, CBM3, and CBM4 at the X point.

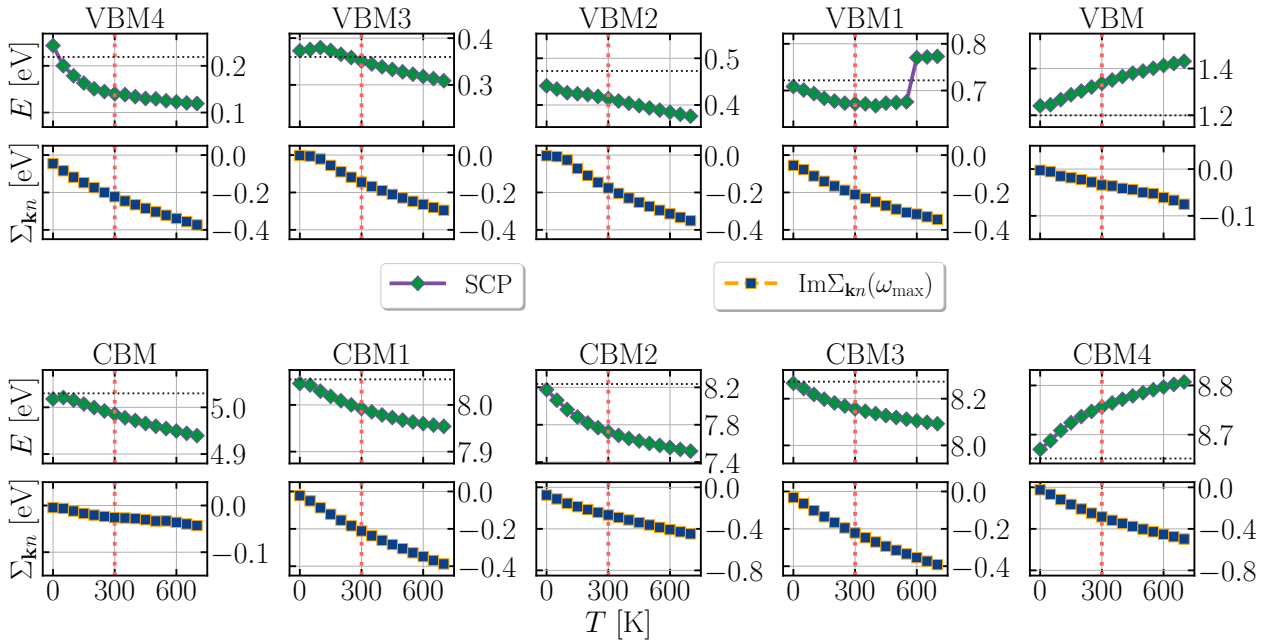

Fig. S64. Temperature dependence of the band energy and the imaginary part of the self-energy for VBM and VBMx (CBM and CBMx) bands (where $x = 1, 2, 3, 4$) calculated using the SCP approach. The results are shown for $CsPbI_3$ at the X point. Vertical and horizontal dotted lines represent the temperature of the phase transition to cubic structure $T_c = 300$ K and band energy from PBE0 calculations, respectively.

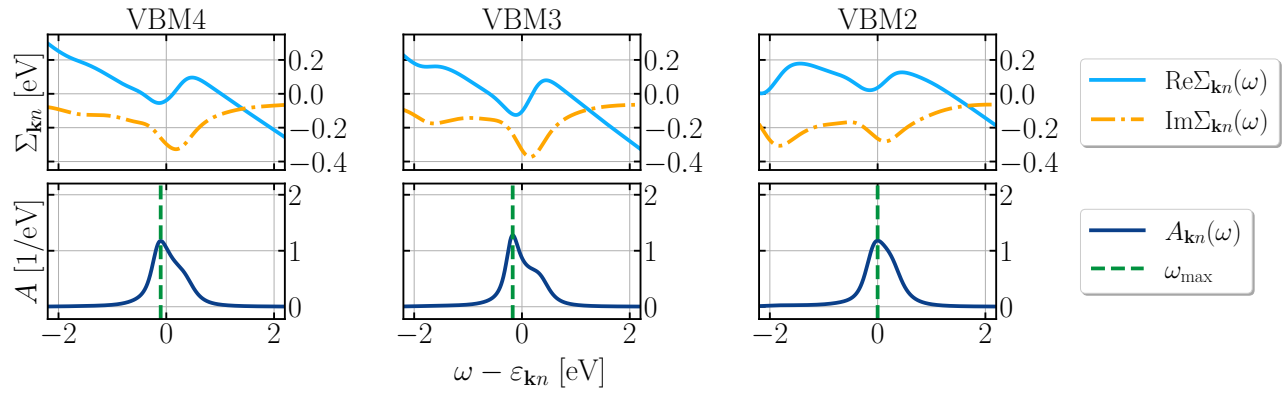

Fig. S65. The frequency dependence of the self-energy and the spectral function for bands VBM4, VBM3, and VBM2 at the M point in the case of $CsPbCl_3$ material at $T = 400$ K.

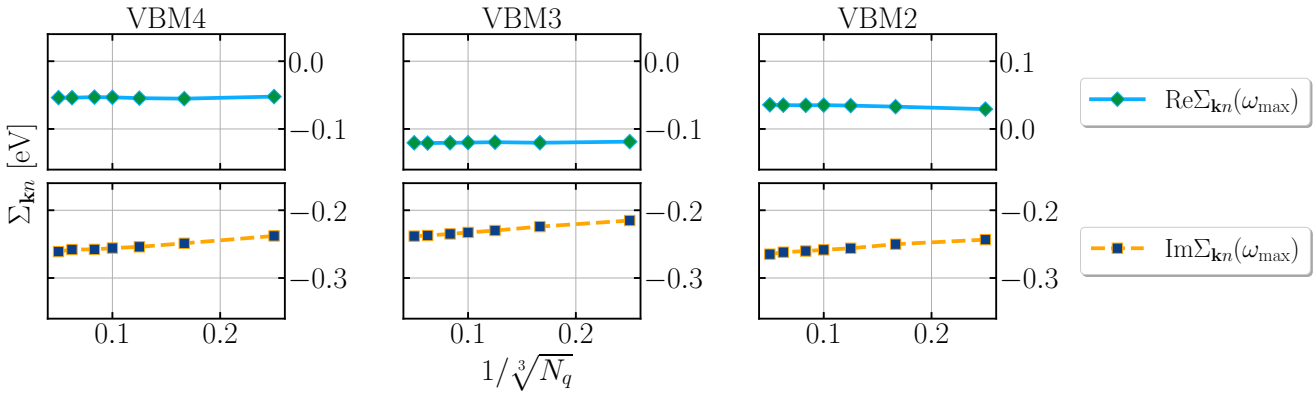

Fig. S66. The dependence of the real and imaginary part of self-energy at the renormalized energy on the size of the q-points grid. The results are presented for $CsPbCl_3$ material at $T = 400$ K for bands VBM4, VBM3, and VBM2 at the M point.

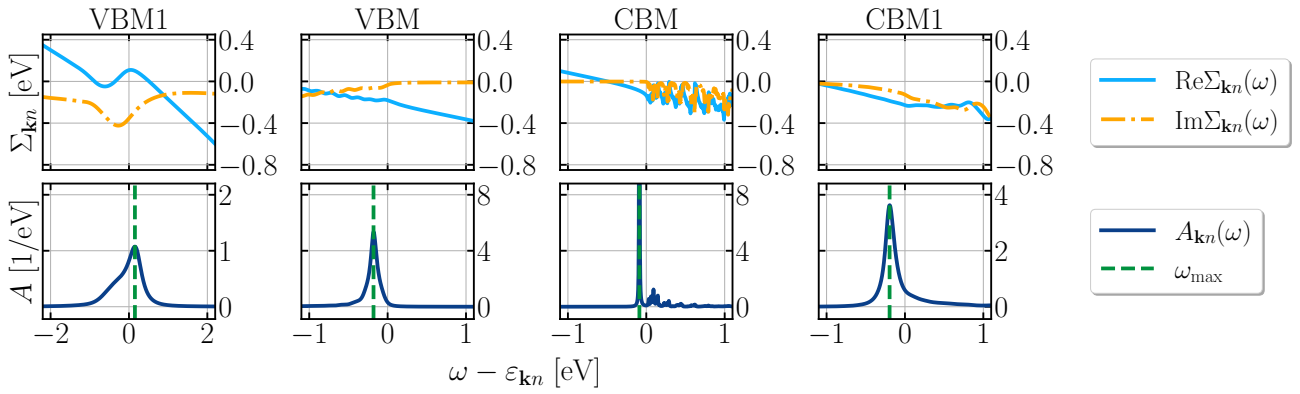

Fig. S67. The frequency dependence of the self-energy and the spectral function for bands VBM1, VBM, CBM and CBM1 at the M point in the case of $CsPbCl_3$ material at $T = 400$ K.

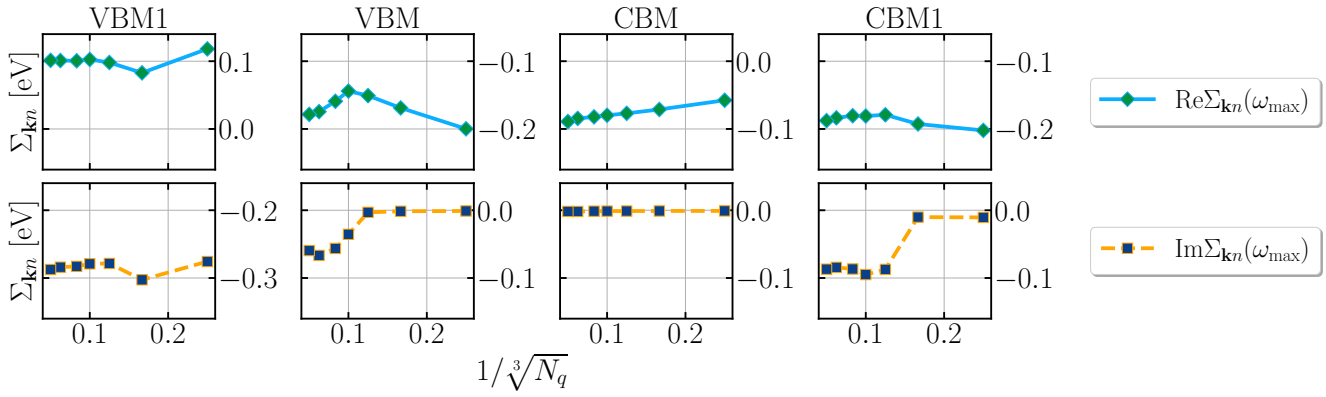

Fig. S68. The dependence of the real and imaginary part of self-energy at the renormalized energy on the size of the q-points grid. The results are presented for $CsPbCl_3$ material at $T = 400$ K for bands VBM1, VBM, CBM and CBM1 at the M point.

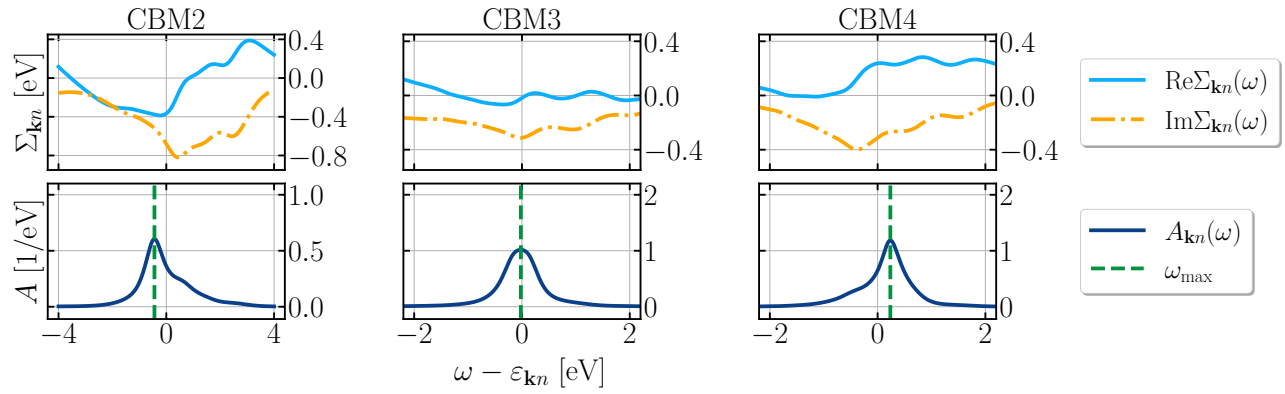

Fig. S69. The frequency dependence of the self-energy and the spectral function for bands CBM2, CBM3, and CBM4 at the M point in the case of $CsPbCl_3$ material at $T = 400$ K.

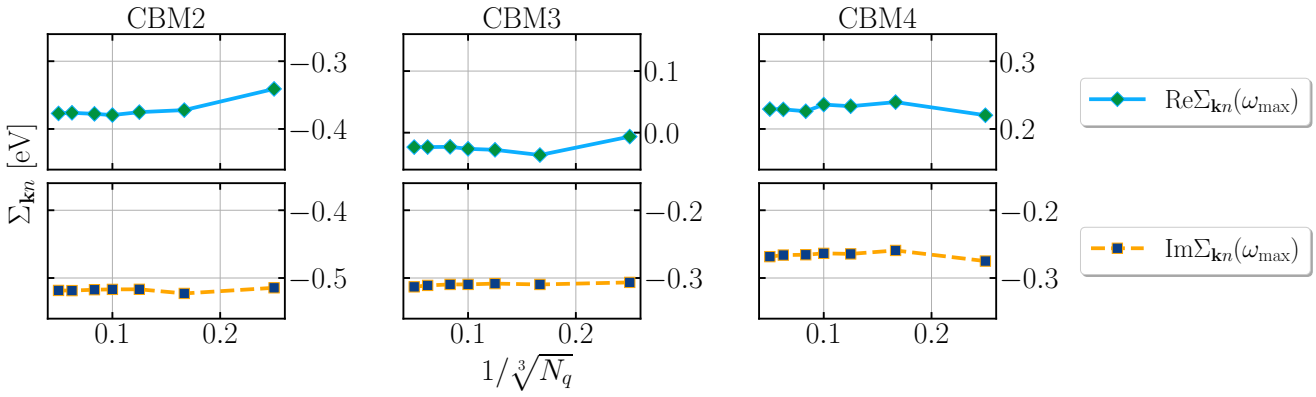

Fig. S70. The dependence of the real and imaginary part of self-energy at the renormalized energy on the size of the q-points grid. The results are presented for $CsPbCl_3$ material at $T = 400$ K for bands CBM2, CBM3, and CBM4 at the M point.

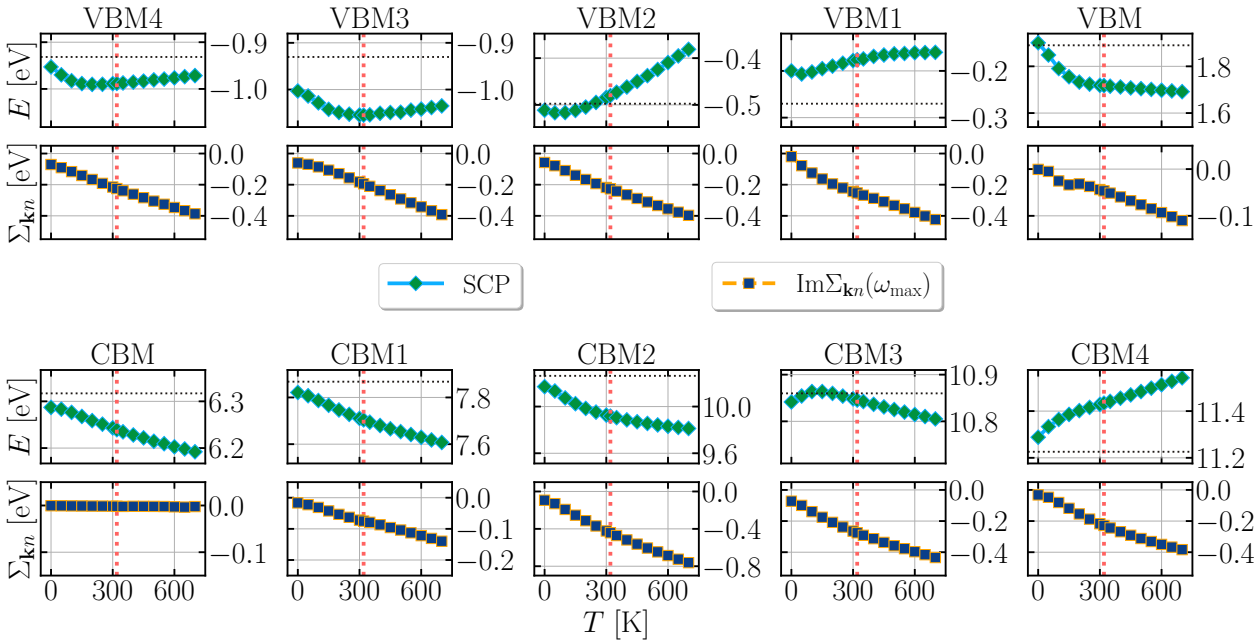

Fig. S71. Temperature dependence of the band energy and the imaginary part of the self-energy for VBM and VBMx (CBM and CBMx) bands (where $x = 1, 2, 3, 4$) calculated using the SCP approach. The results are shown for $CsPbCl_3$ at the M point. Vertical and horizontal dotted lines represent the temperature of the phase transition to cubic structure $T_c = 320$ K and band energy from PBE0 calculations, respectively.

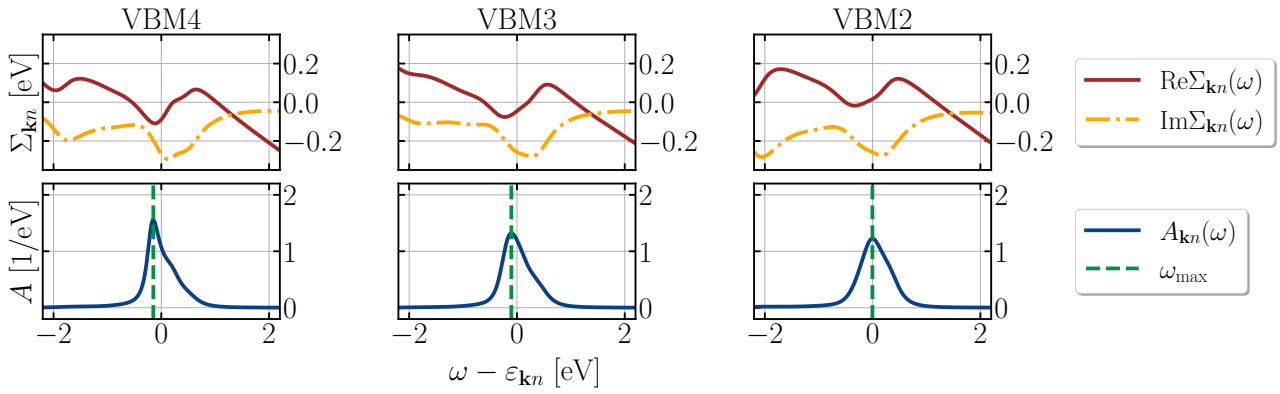

Fig. S72. The frequency dependence of the self-energy and the spectral function for bands VBM4, VBM3, and VBM2 at the M point in the case of $CsPbBr_3$ material at $T = 400$ K.

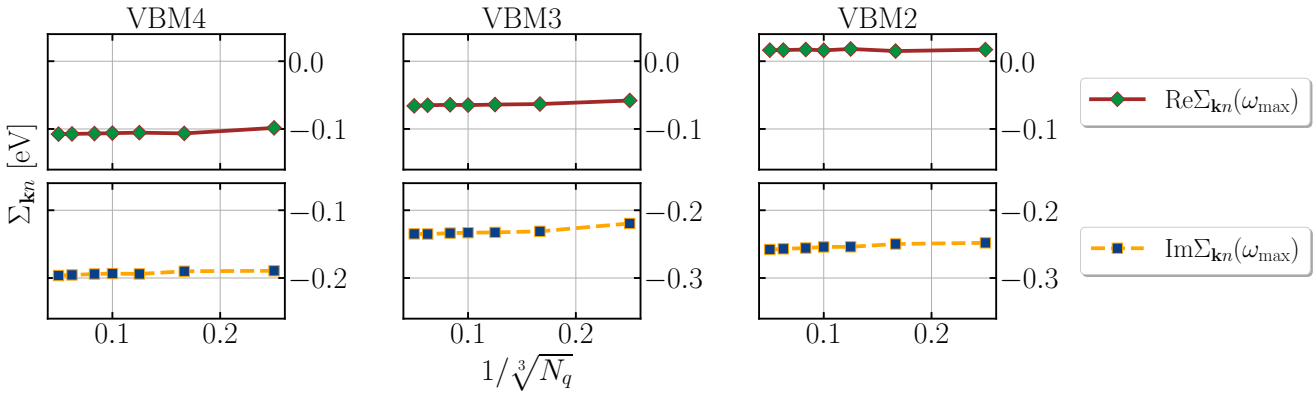

Fig. S73. The dependence of the real and imaginary part of self-energy at the renormalized energy on the size of the q-points grid. The results are presented for $CsPbBr_3$ material at $T = 400$ K for bands VBM4, VBM3, and VBM2 at the M point.

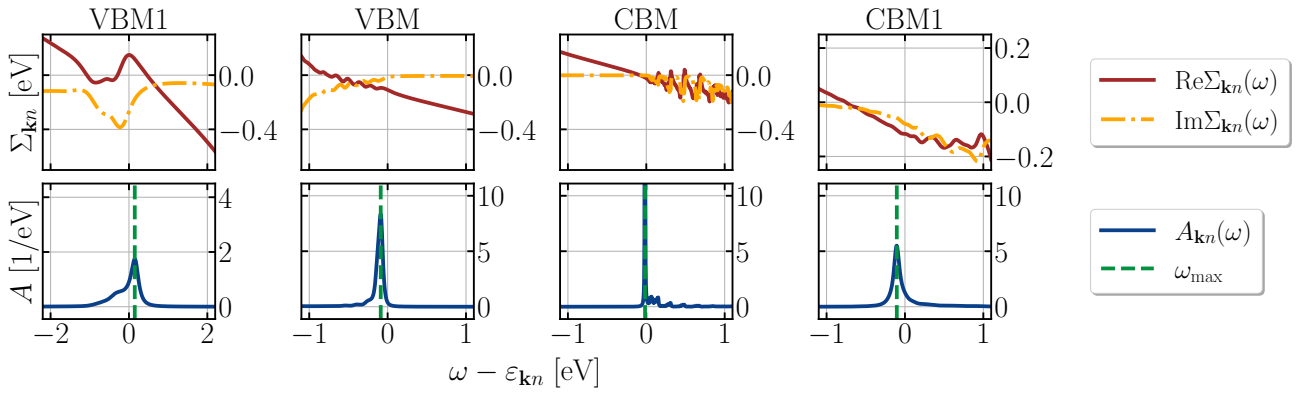

Fig. S74. The frequency dependence of the self-energy and the spectral function for bands VBM1, VBM, CBM and CBM1 at the M point in the case of $CsPbBr_3$ material at $T = 400$ K.

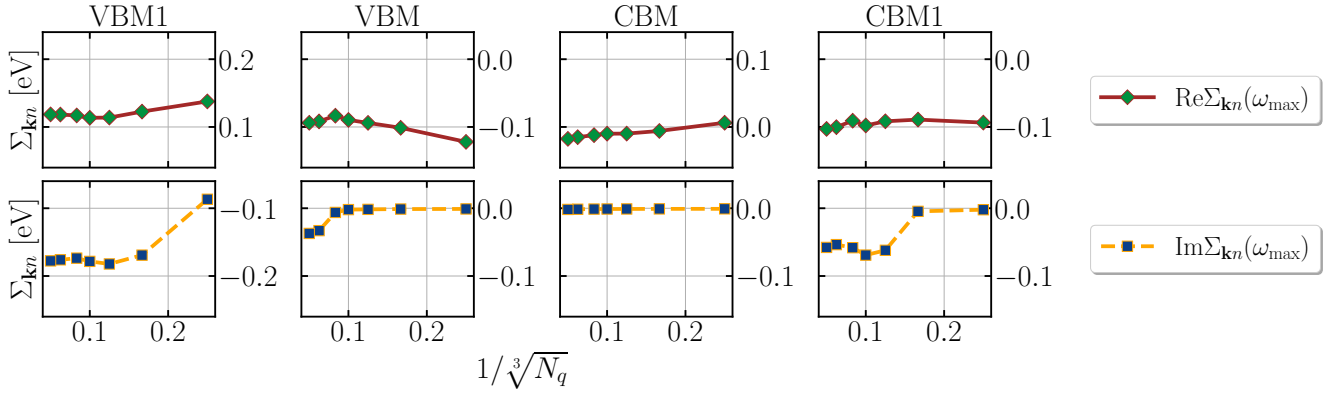

Fig. S75. The dependence of the real and imaginary part of self-energy at the renormalized energy on the size of the q-points grid. The results are presented for $CsPbBr_3$ material at $T = 400$ K for bands VBM1, VBM, CBM and CBM1 at the M point.

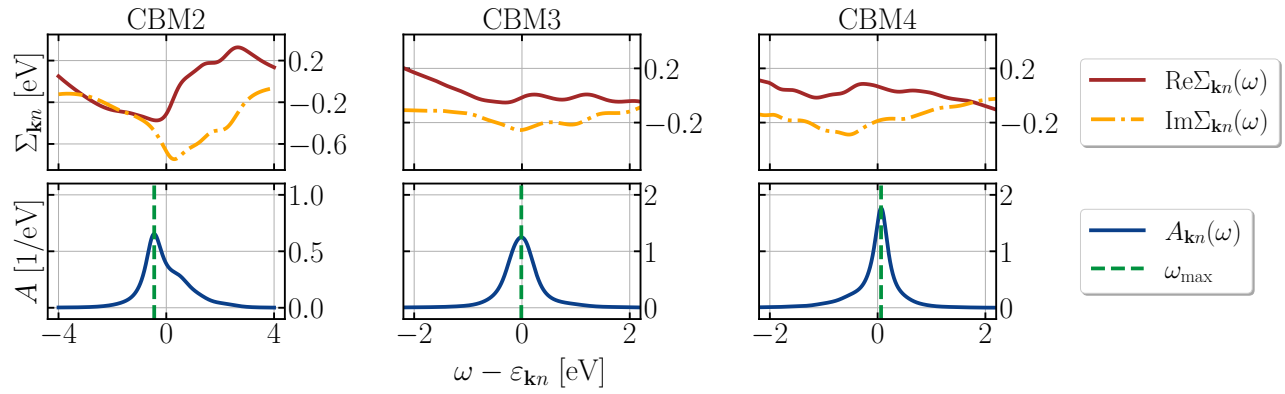

Fig. S76. The frequency dependence of the self-energy and the spectral function for bands CBM2, CBM3, and CBM4 at the M point in the case of $CsPbBr_3$ material at $T = 400$ K.

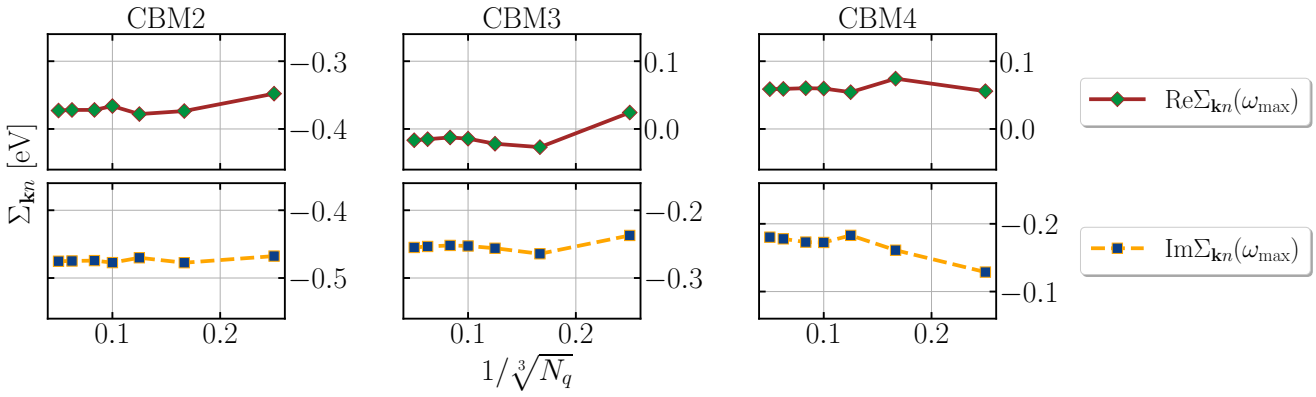

Fig. S77. The dependence of the real and imaginary part of self-energy at the renormalized energy on the size of the q-points grid. The results are presented for $CsPbBr_3$ material at $T = 400$ K for bands CBM2, CBM3, and CBM4 at the M point.

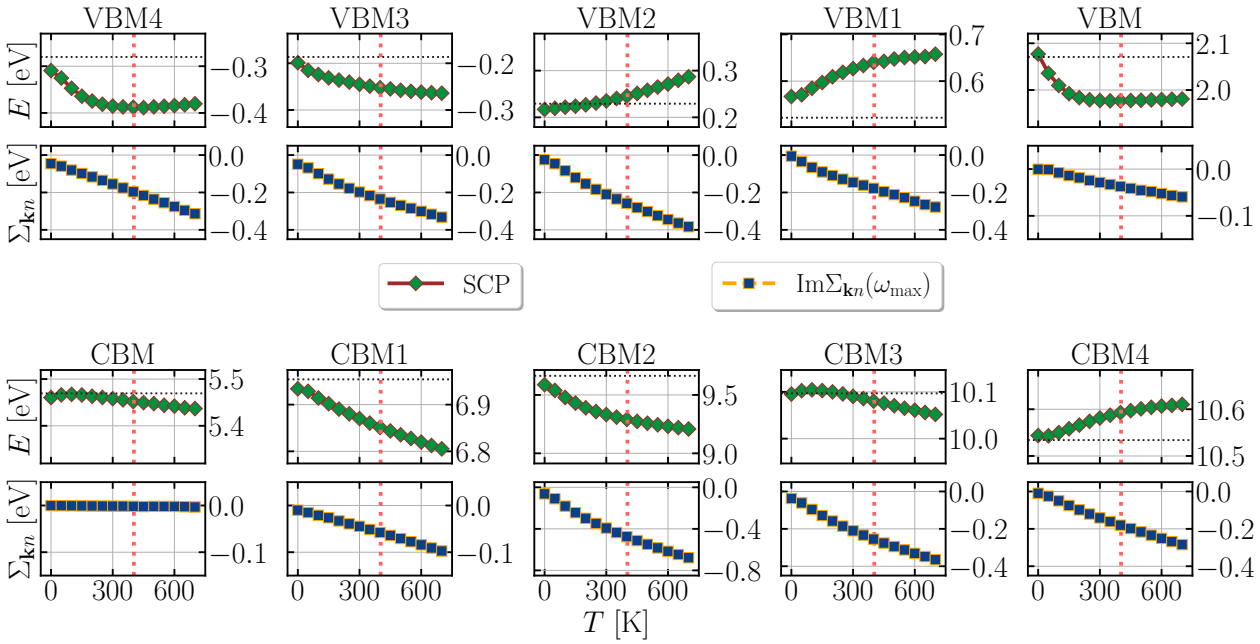

Fig. S78. Temperature dependence of the band energy and the imaginary part of the self-energy for VBM and VBMx (CBM and CBMx) bands (where $x = 1, 2, 3, 4$) calculated using the SCP approach. The results are shown for $CsPbBr_3$ at the M point. Vertical and horizontal dotted lines represent the temperature of the phase transition to cubic structure $T_c = 403\,K$ and band energy from PBE0 calculations, respectively.

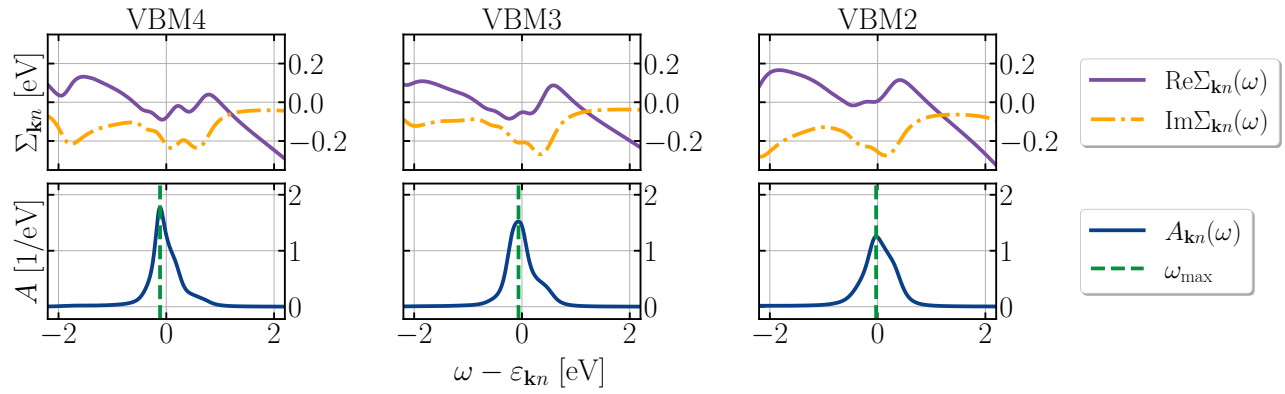

Fig. S79. The frequency dependence of the self-energy and the spectral function for bands VBM4, VBM3, and VBM2 at the M point in the case of $CsPbI_3$ material at $T = 400$ K.

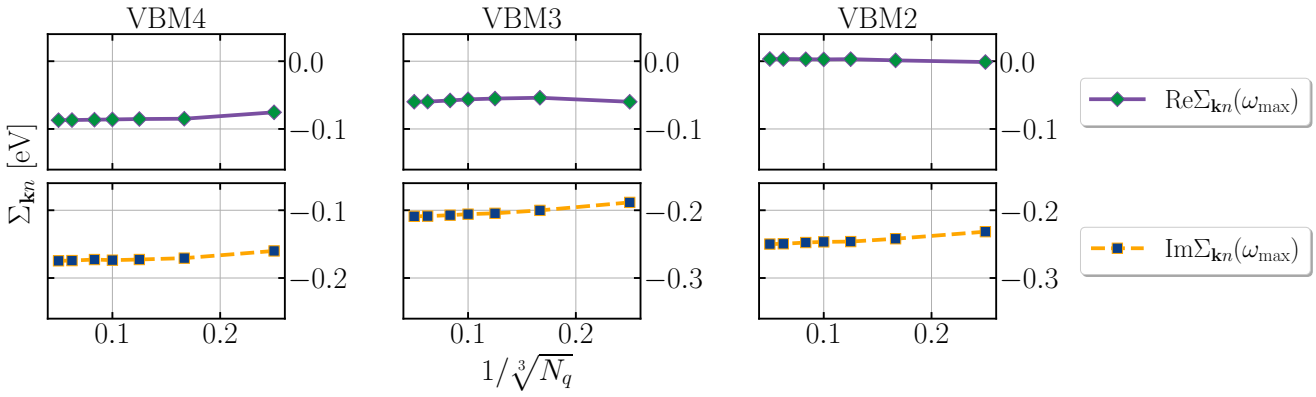

Fig. S80. The dependence of the real and imaginary part of self-energy at the renormalized energy on the size of the q-points grid. The results are presented for $CsPbI_3$ material at $T = 400$ K for bands VBM4, VBM3, and VBM2 at the M point.

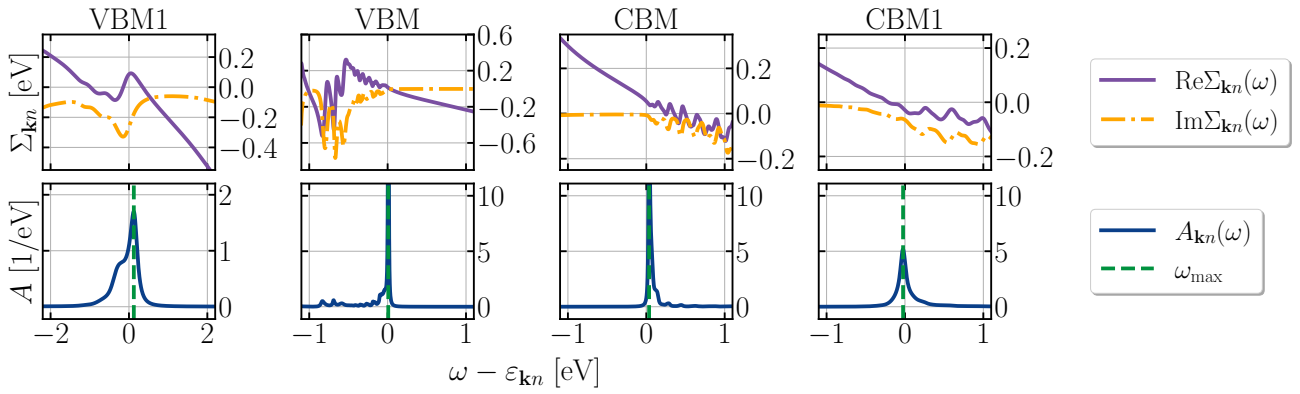

Fig. S81. The frequency dependence of the self-energy and the spectral function for bands VBM1, VBM, CBM and CBM1 at the M point in the case of $CsPbI_3$ material at $T = 400$ K.

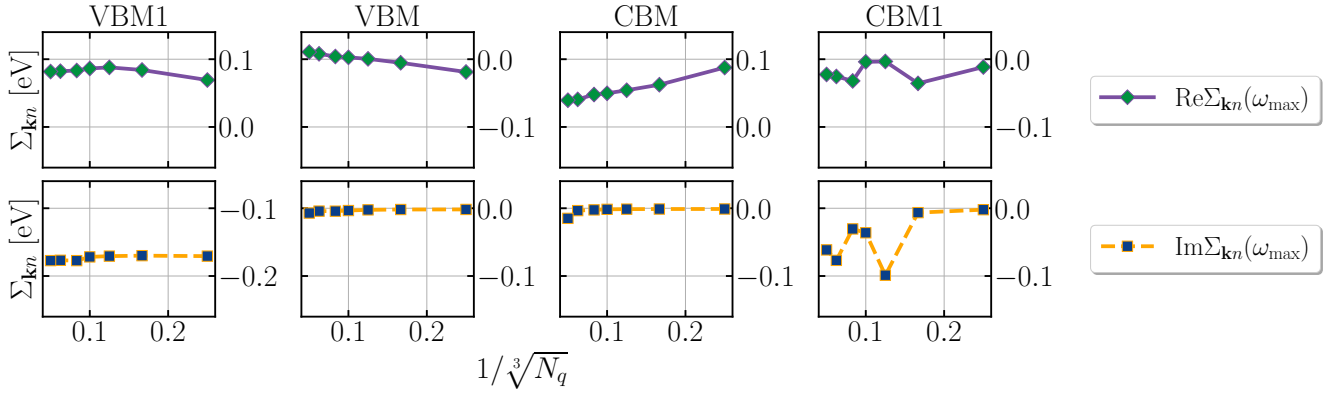

Fig. S82. The dependence of the real and imaginary part of self-energy at the renormalized energy on the size of the q-points grid. The results are presented for $CsPbI_3$ material at $T = 400$ K for bands VBM1, VBM, CBM and CBM1 at the M point.

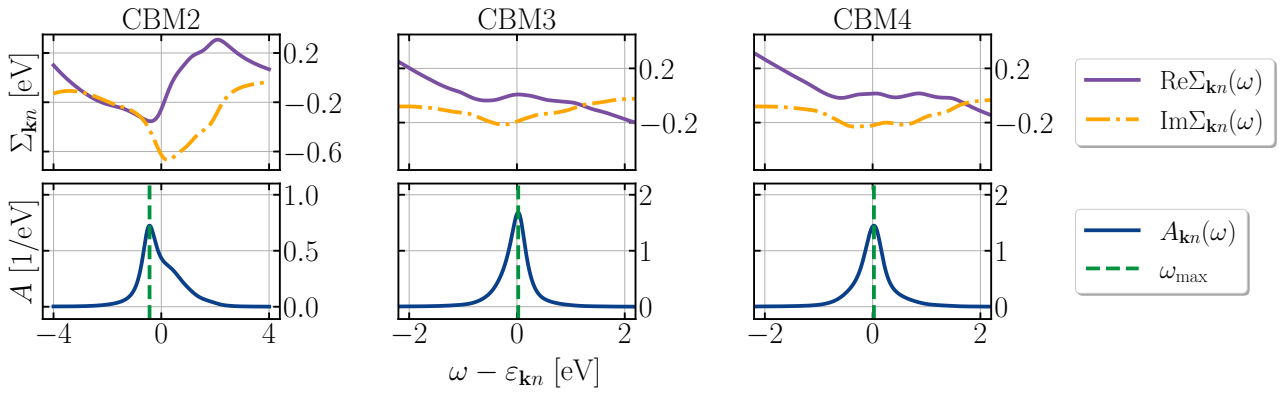

Fig. S83. The frequency dependence of the self-energy and the spectral function for bands CBM2, CBM3, and CBM4 at the M point in the case of $CsPbI_3$ material at $T = 400\,\mathrm{K}$.

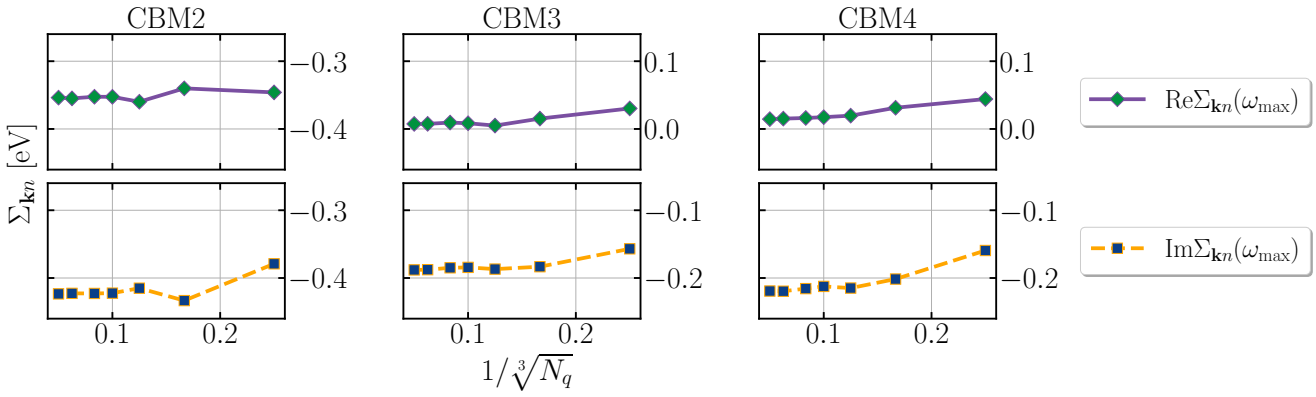

Fig. S84. The dependence of the real and imaginary part of self-energy at the renormalized energy on the size of the q-points grid. The results are presented for $CsPbI_3$ material at $T = 400\,\mathrm{K}$ for bands CBM2, CBM3, and CBM4 at the M point.

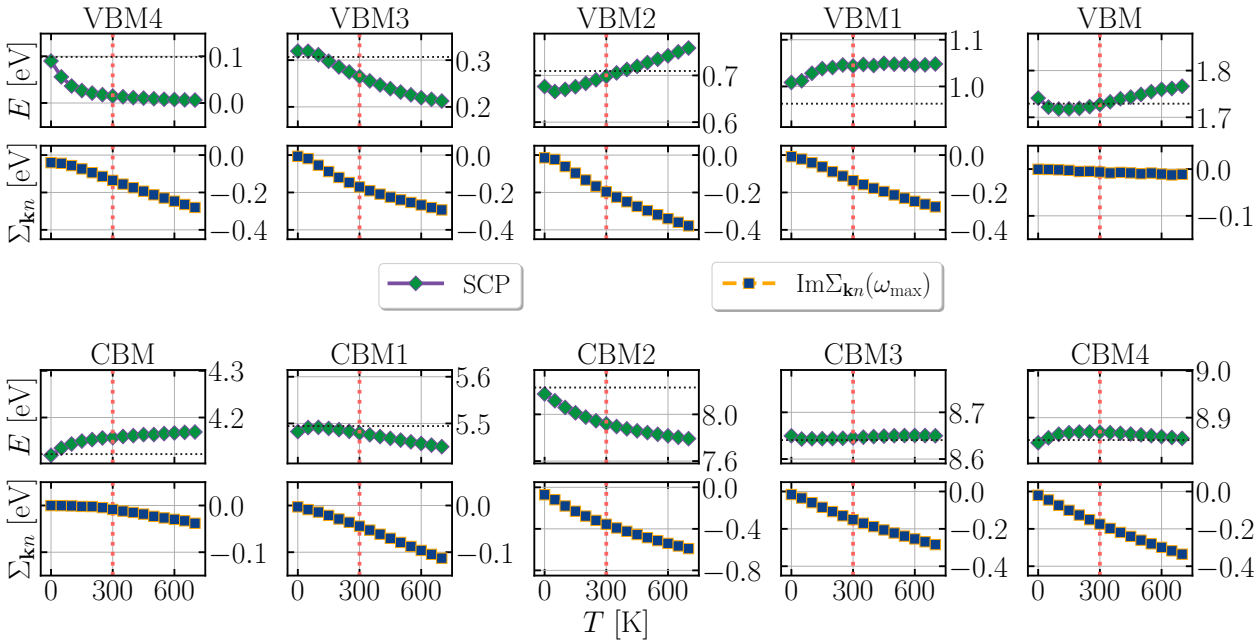

Fig. S85. Temperature dependence of the band energy and the imaginary part of the self-energy for VBM and VBMx (CBM and CBMx) bands (where $x = 1, 2, 3, 4$) calculated using the SCP approach. The results are shown for $CsPbI_3$ at the M point. Vertical and horizontal dotted lines represent the temperature of the phase transition to cubic structure $T_c = 300$ K and band energy from PBE0 calculations, respectively.

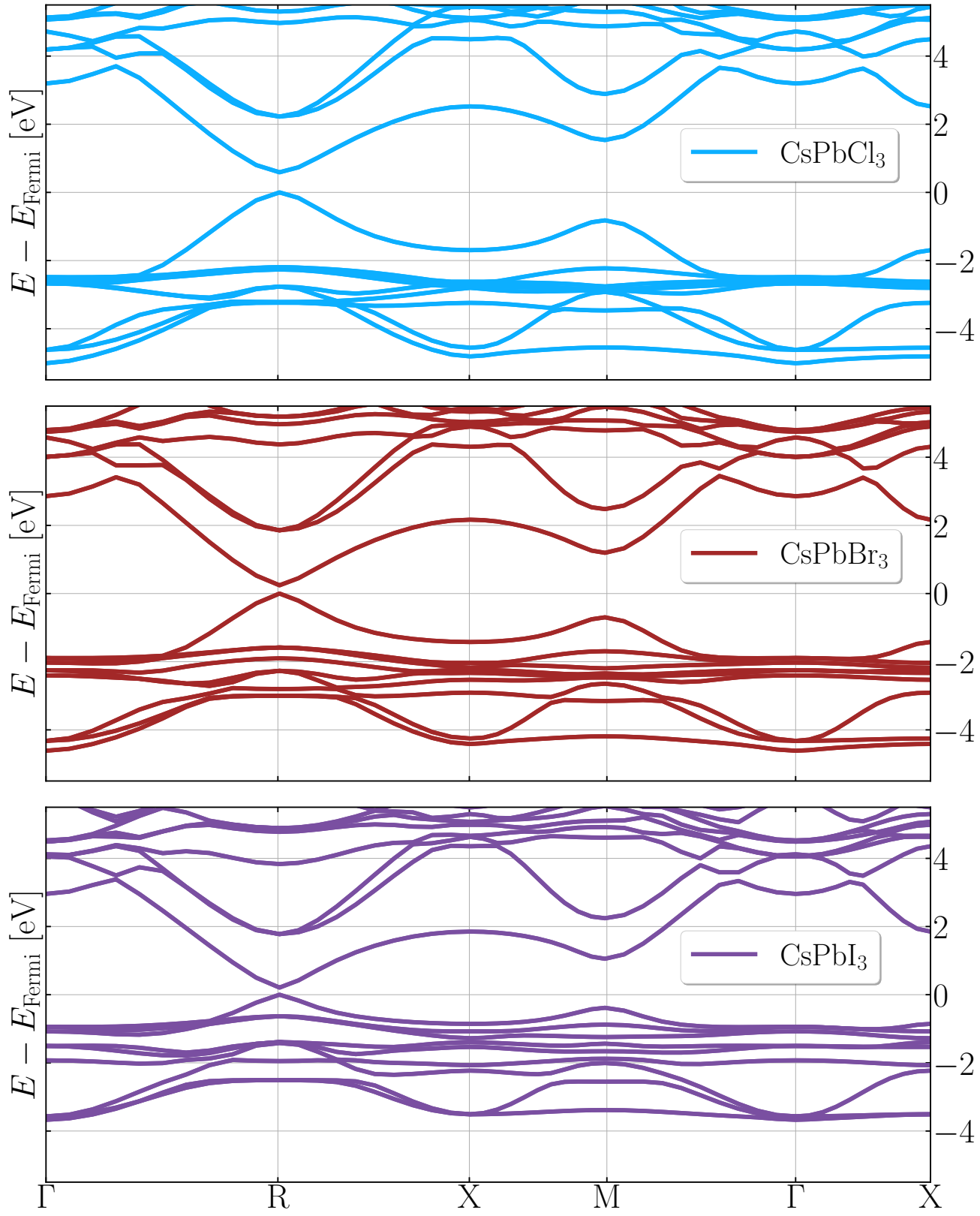

Fig. S86. Electronic band structure obtained from DFT using PBEsol functional for $CsPbCl_3$ and $CsPbBr_3$, and PBE functional for $CsPbI_3$.

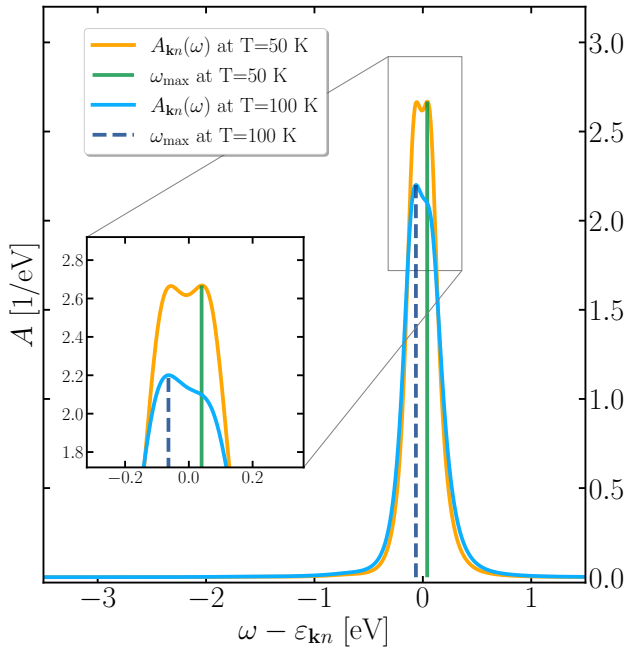

Fig. S87. Spectral function of $CsPbCl_3$ at $T = 50$ K and $T = 100$ K for VBM2 band at the X point. The inset shows zoomed figure around the peaks to show the shift of spectral function maximum with temperature.

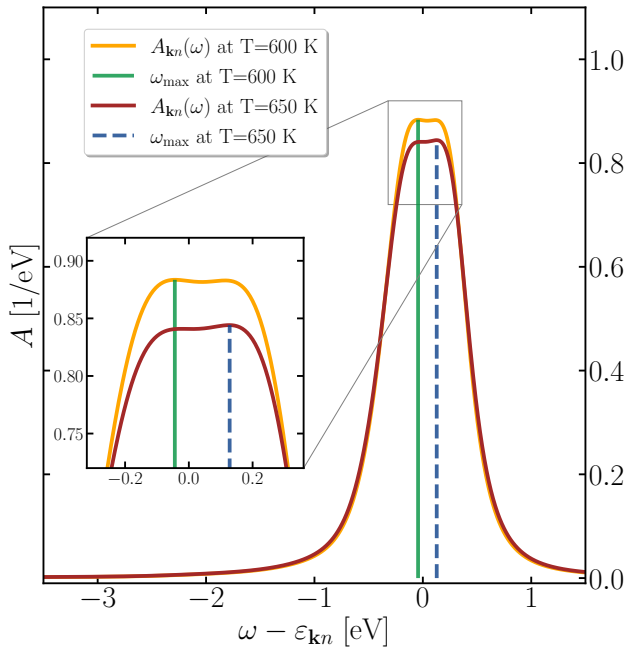

Fig. S88. Spectral function of $CsPbBr_3$ at $T = 600$ K and $T = 650$ K for VBM1 band at the X point. The inset shows zoomed figure around the peaks to show the shift of spectral function maximum with temperature.

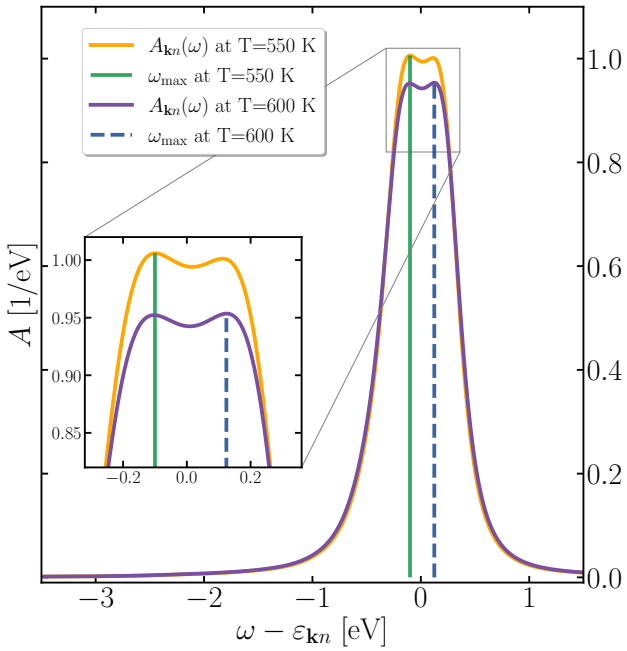

Fig. S89. Spectral function of $CsPbI_3$ at $T = 550$ K and $T = 600$ K for VBM1 band at the X point. The inset shows zoomed figure around the peaks to show the shift of spectral function maximum with temperature.